Climate-Driven Stochastic Modelling of Crimean-Congo Haemorrhagic Fever Transmission in Uganda

P. G. Kpatchana[1]*, J. Aduda[2], K. M. Agboka[3]

[1]Pan African University Institute for Basic Sciences, Technology and Innovation (PAUSTI), Nairobi, Kenya.
[2]Department of Statistics and Actuarial Science, Jomo Kenyatta University of Agriculture and Technology (JKUAT), Nairobi, Kenya.
[3]Climate Risk Data Scientist, Integrated Data and Analytics Platform (IDAP), International Centre of Insect Physiology and Ecology (ICIPE), Nairobi, Kenya.

ABSTRACT: Crimean-Congo haemorrhagic fever (CCHF) is a climate-sensitive tick-borne zoonosis that remains a significant public health concern in Uganda, where temperature and vapour pressure deficit influence tick ecology and consequently disease transmission. This study aimed to develop and analyse a climate-driven stochastic model for CCHF transmission among ticks, livestock, and humans under environmental variability in Uganda. A compartmental transmission model was formulated and extended into a stochastic differential equation framework by incorporating multiplicative environmental noise. Climate-dependent tick recruitment, development, and mortality were parameterized using district-level temperature and vapour pressure deficit data to capture spatial heterogeneity in transmission risk. Theoretical analyses based on the next-generation matrix, Lyapunov methods, and stochastic stability theory were used to derive the basic reproduction number and establish positivity, boundedness, equilibrium stability, extinction conditions, and the existence of a stationary distribution and ergodicity. Numerical simulations were performed using the Milstein scheme over a three-year period to compare deterministic and stochastic dynamics under endemic and sub-threshold transmission scenarios, while district-level climate data were used to generate spatial risk maps and evaluate model performance against reported CCHF outbreaks. The model reproduced seasonal transmission patterns, predicted rapid disease extinction under sub-threshold conditions, and persistent endemic dynamics when $R_0 > 1$. Spatial analyses revealed substantial geographical variation in transmission potential, and model validation achieved a classification accuracy of 79.6% against reported outbreak districts. The proposed framework provides a practical tool for climate-informed CCHF surveillance, spatial risk assessment, early warning, and prioritization of targeted intervention strategies in Uganda.

KEYWORDS: Crimean-Congo haemorrhagic fever, stochastic differential equations, Climate-driven transmission, Hyalomma ticks, Basic reproduction number, Uganda.

[Received May 24, 2026; Revised Jun. 19, 2026; Accepted Jun. 22, 2026] Print ISSN: 0189-9546 | Online ISSN: 2437-2110

I. INTRODUCTION

Crimean-Congo haemorrhagic fever (CCHF) is a zoonotic viral disease of major public health importance in Africa, Asia, the Middle East, and parts of Europe (Bernard et al., 2022; World Health Organization, 2025). The disease is caused by the Crimean-Congo haemorrhagic fever virus and is primarily transmitted by infected ticks, particularly those of the Hyalomma genus (Bernard et al., 2022; World Health Organization, 2025). In addition to vector-borne transmission, humans may become infected through direct contact with infected livestock or through exposure to contaminated blood and body fluids from infected individuals. Because of these multiple transmission pathways, CCHF represents a complex epidemiological system involving vectors, animal hosts, and humans. The disease has attracted increasing attention due to its high case fatality rate, recurrent outbreaks, and potential for geographical expansion under changing climatic conditions.

Ticks play a central role in maintaining and amplifying CCHF transmission. Their development, survival, reproduction, and host-seeking behaviour are highly sensitive to environmental conditions, particularly temperature and atmospheric moisture (Randolph & Rogers, 2007; Estrada-Peña, Martínez Avilés & Muñoz Reoyo, 2011; Estrada-Peña, 2023). Climatic variability directly influences tick abundance, developmental duration, mortality, and contact rates with livestock and humans. Seasonal environmental changes may therefore produce substantial fluctuations in transmission intensity and disease risk. These characteristics make CCHF particularly suitable for climate-informed mathematical modelling.

Temperature alone does not fully characterize the environmental constraints experienced by ticks. Moisture availability is equally important because ticks are highly susceptible to desiccation during off-host periods. While relative humidity is commonly used in ecological studies, vapor pressure deficit (VPD) provides a more direct measure of atmospheric drying power and therefore better reflects the moisture stress experienced by ticks. Previous ecological investigations have demonstrated that tick survival, questing activity, and developmental success are strongly influenced by atmospheric moisture deficits represented by VPD,

*Corresponding author: piham.kpatchana@students.jkuat.ac.ke
doi: http://doi.org/10.63746/njtd.v23i2.4823

making it a biologically meaningful predictor for climate-driven tick population modelling (Randolph & Rogers, 2007; Estrada-Peña et al., 2011; Estrada-Peña, 2023). Consequently, temperature and VPD were selected as the principal environmental drivers in the present study.

Mathematical models have long been used to investigate infectious disease transmission, evaluate intervention strategies, and determine threshold conditions for disease persistence or elimination (Hethcote, 2000; Van den Driessche & Watmough, 2002). Deterministic compartmental models are particularly useful for describing average disease dynamics, deriving threshold quantities such as the basic reproduction number, and analysing equilibrium stability. However, deterministic formulations typically assume fixed parameter values and homogeneous environmental conditions, which may not adequately capture the variability observed in real epidemiological systems.

Stochastic epidemic models provide a more realistic framework when disease transmission is influenced by environmental fluctuations and demographic uncertainty. By incorporating random perturbations into epidemiological rates and population dynamics, stochastic differential equation models allow the investigation of persistence, extinction, long-term disease behaviour, and uncertainty propagation under varying environmental conditions (Mao, 2007; Allen, 2008). Such considerations are particularly relevant for CCHF because climatic variability affects tick mortality, development, reproduction, and infection pressure in ways that cannot be fully represented by deterministic formulations alone.

Several mathematical models of CCHF transmission have been proposed in the literature, including deterministic compartmental models and climate-sensitive vector population models (Estrada-Peña et al., 2011; Bhowmick et al., 2022). Nevertheless, most existing studies either neglect environmental stochasticity or focus primarily on vector ecology without explicitly linking climate-driven tick dynamics to epidemiological transmission among ticks, livestock, and humans. Furthermore, few studies have examined climate-driven transmission risk at district level in Uganda despite the country's ecological diversity and recurrent occurrence of CCHF outbreaks. These limitations motivate the development of an integrated stochastic modelling framework capable of capturing both environmental variability and spatial heterogeneity in transmission potential.

Spatial heterogeneity plays an important role in shaping CCHF transmission dynamics. Climatic conditions, livestock density, ecological suitability, and human exposure vary considerably across geographical regions and directly influence vector abundance and disease risk. In Uganda, environmental conditions differ substantially among districts and agroecological zones, resulting in spatially varying transmission potential (Omoga et al., 2023; Balinandi et al., 2024; Zalwango et al., 2024). A modelling framework that links climate-dependent tick dynamics with district-level epidemiological indicators provides a practical approach for assessing spatial and seasonal transmission risk and for supporting climate-informed surveillance strategies.

Motivated by these considerations, this study develops a climate-driven stochastic model of CCHF transmission based on tick–livestock–human interactions in Uganda. The deterministic component describes disease progression among susceptible, exposed, infectious, and recovered populations, while the stochastic formulation introduces multiplicative Brownian perturbations representing environmental variability and uncertainty. Climate dependent tick demographic parameters are incorporated through temperature and vapor pressure deficit data, and district-level climatic conditions are used to characterize spatial heterogeneity in transmission potential. In addition, deterministic and stochastic model predictions are compared to evaluate the epidemiological implications of environmental variability and to quantify the additional insights provided by stochastic modelling.

The main contributions of this study are summarized as follows:

i. Development of a stochastic CCHF transmission model integrating tick–livestock–human interactions under environmental variability.
ii. Incorporation of climate-dependent tick demographic parameters driven by temperature and vapor pressure deficit.
iii. Analytical characterization of positivity, disease-free equilibrium stability, extinction conditions, stationary distribution, and ergodicity properties.
iv. Comparison of deterministic and stochastic climate-driven transmission dynamics to evaluate the contribution of environmental stochasticity.
v. Spatial mapping of climate-driven transmission potential and associated uncertainty across Uganda at district level.
vi. Integration of stochastic disease dynamics with climate-sensitive tick lifecycle modelling to support climate-informed surveillance and risk assessment.

The remainder of this paper is organized as follows. Section II presents the theoretical formulation of the deterministic and stochastic models. Section III describes the study area, climate datasets, and computational methodology. Section IV presents and discusses the numerical and spatial results. Finally, Section V concludes the study and highlights directions for future research.

II. THEORETICAL FRAMEWORK

A. Model Structure and Assumptions

The proposed model describes the transmission dynamics of Crimean-Congo Haemorrhagic Fever (CCHF) through interactions among three epidemiological populations: ticks (vector), livestock (amplifying host), and humans (spillover host). The formulation is based on a compartmental structure that captures both the biological progression of infection and the ecological role of each population (Bhowmick *et al.*, 2022).

The following assumptions underlie the model formulation:

i. Homogeneous mixing: Individuals within each population mix uniformly, and contacts between ticks, livestock, and humans occur at average rates.
ii. Climate-driven vector dynamics: Tick recruitment, mortality, and developmental rates are influenced by temperature and vapor pressure deficit.
iii. Multi-route transmission: Infection may occur through livestock-to-tick, tick-to-tick, tick-to-livestock, tick-to-human, livestock-to-human, and human-to-human transmission.
iv. Latent infection stage: Livestock and humans pass through an exposed stage before becoming infectious.

v. Temporary immunity: Recovered humans may lose immunity and return to the susceptible class.
vi. Vertical transmission: A proportion of newly recruited ticks may be infected at birth.
vii. Environmental stochasticity: Climatic variability is represented through multiplicative stochastic perturbations.
viii. Spatial heterogeneity: Climatic conditions vary across districts, leading to geographically varying transmission potential.

B. Deterministic Climate-Driven Model

The human population is partitioned into susceptible, exposed, infectious, and recovered compartments denoted by $H_S(t), H_E(t)$, $H_I(t)$ and $H_R(t)$, respectively. The livestock population is partitioned into $L_S(t), L_E(t)$, $L_I(t)$ and $L_R(t)$, while the tick population is represented by $T_S(t), T_E(t)$ and $T_I(t)$. Table 1 describe the parameters used in the model.

Total populations are defined as

$$N_H = H_S + H_E + H_I + H_R \quad (1)$$
$$N_L = L_S + L_E + L_I + L_R \quad (2)$$
$$N_T = T_S + T_E + T_I \quad (3)$$

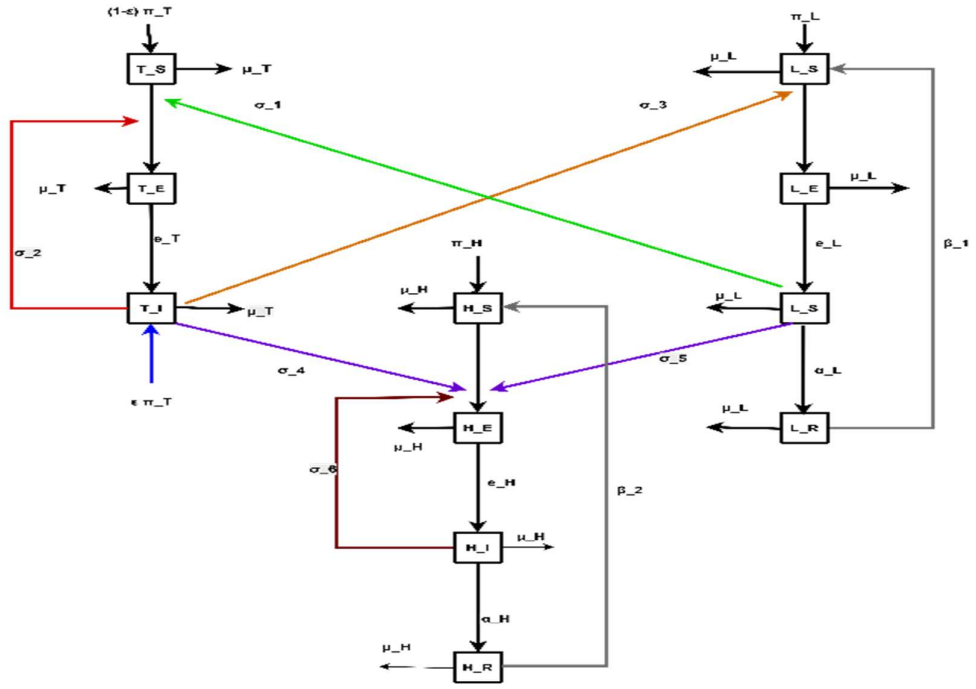

Figure 1 Compartmental structure of the proposed CCHF transmission model illustrating interactions between tick, livestock, and human populations. Arrows represent transmission pathways and progression between epidemiological states.

The deterministic dynamics are described by:

i) Human population

$$\frac{dH_S}{dt} = \pi_H - \frac{\sigma_4 H_S T_I}{N_T} - \frac{\sigma_5 H_S L_I}{N_L} - \frac{\sigma_6 H_S H_I}{N_H} - \mu_H H_S + \omega H_R \quad (4)$$

$$\frac{dH_E}{dt} = \frac{\sigma_4 H_S T_I}{N_T} + \frac{\sigma_5 H_S L_I}{N_L} + \frac{\sigma_6 H_S H_I}{N_H} - e_H H_E - \mu_H H_E \quad (5)$$

$$\frac{dH_I}{dt} = e_H H_E - (\alpha_H + \mu_H + \delta_H) H_I \quad (6)$$

$$\frac{dH_R}{dt} = \alpha_H H_I - (\mu_H + \omega) H_R \quad (7)$$

ii) Livestock population

$$\frac{dL_S}{dt} = \pi_L - \frac{\sigma_3 L_S T_I}{N_T} - \mu_L L_S \quad (8)$$

$$\frac{dL_E}{dt} = \frac{\sigma_3 L_S T_I}{N_T} - e_L L_E - \mu_L L_E \quad (9)$$

$$\frac{dL_I}{dt} = e_L L_E - (\alpha_L + \mu_L) L_I \quad (10)$$

$$\frac{dL_R}{dt} = \alpha_L L_I - \mu_L L_R \quad (11)$$

iii) Tick population

$$\frac{dT_S}{dt} = \pi_T \left(1 - \frac{\varepsilon T_I}{N_T}\right) - \frac{\sigma_1 T_S L_I}{N_L} - \frac{\sigma_2 T_S T_I}{N_T} - \mu_T T_S \quad (12)$$

$$\frac{dT_E}{dt} = \frac{\sigma_1 T_S L_I}{N_L} + \frac{\sigma_2 T_S T_I}{N_T} - (\mu_T + e_T) T_E \quad (13)$$

$$\frac{dT_I}{dt} = \frac{\varepsilon \pi_T T_I}{N_T} + e_T T_E - \mu_T T_I \quad (14)$$

Table 1 Model parameters

Parameter	Description
π_H, π_L, π_T	Human recruitment, Livestock recruitment and Tick recruitment respectively
μ_H, μ_L, μ_T	Human natural death, Livestock natural death and Tick natural death respectively
$\sigma_1, \sigma_2, \sigma_3, \sigma_4, \sigma_5, \sigma_6$	Livestock-to-tick, Tick-to-tick, Tick-to-livestock, Tick-to-human, Livestock-to-human, Human-to-human transmission
(e_H, e_L, e_T)	Progression rates
(α_H, α_L)	Recovery rates
(δ_H)	Human disease mortality
(ω)	Immunity loss
(ε)	Vertical transmission

C. Stochastic Model Formulation

To account for environmental variability and uncertainty in CCHF transmission dynamics, the deterministic model is extended into a stochastic framework. This extension is motivated by the fact that key epidemiological processes, particularly those related to tick survival, development, and host interaction, are strongly influenced by fluctuating climatic conditions.

Stochastic perturbations are introduced in the form of multiplicative white noise, which reflects proportional environmental variability affecting population sizes and transmission processes. This choice ensures that the intensity of fluctuations scales with the magnitude of the state variables, thereby preserving biological realism. The stochastic formulation is derived using Itô stochastic differential equations, where independent Wiener processes represent random environmental forcing.

Let

$$X(t) = (T_S, T_E, T_I, L_S, L_E, L_I, L_R, H_S, H_E, H_I, H_R)^T$$

denote the state vector. Environmental variability is incorporated through compartment-specific diffusion terms $\eta_i X_i dW_i$, where η_i denotes the stochastic intensity associated with compartment X_i and W_i(t) represents an independent Wiener process. Consequently, stochastic fluctuations act on the tick, livestock, and human population compartments and scale proportionally with their population sizes.

This approach allows the model to capture irregular epidemic patterns, extinction events, and variability in transmission intensity that cannot be reproduced by deterministic models alone.

The stochastic noise intensities and Wiener processes appearing in the stochastic system are described in Table 2

Accordingly, the stochastic CCHF transmission model is represented by the following system of Itô stochastic differential equations:

$$dT_S = \left[\pi_T\left(1 - \frac{\varepsilon T_I}{N_T}\right) - \frac{\sigma_1 T_S L_I}{N_L} - \frac{\sigma_2 T_S T_I}{N_T} - \mu_T T_S\right] dt + \eta_{TS} T_S\, dW_1 \quad (15)$$

$$dT_E = \left[\frac{\sigma_1 T_S L_I}{N_L} + \frac{\sigma_2 T_S T_I}{N_T} - (\mu_T + e_T) T_E\right] dt + \eta_{T_E} T_E dW_2 \quad (16)$$

$$dT_I = \left[\frac{\varepsilon \pi_T T_I}{N_T} + e_T T_E - \mu_T T_I\right] dt + \eta_{TI} T_I\, dW_3 \quad (17)$$

$$dL_S = \left[\pi_L - \frac{\sigma_3 L_S T_I}{N_T} - \mu_L L_S\right] dt + \eta_{L_S} L_S dW_4 \quad (18)$$

$$dL_E = \left[\frac{\sigma_3 L_S T_I}{N_T} - (e_L + \mu_L) L_E\right] dt + \eta_{L_E} L_E dW_5 \quad (19)$$

$$dL_I = [e_L L_E - (\alpha_L + \mu_L) L_I] dt + \eta_{L_I} L_I dW_6 \quad (20)$$

$$dL_R = [\alpha_L L_I - \mu_L L_R] dt + \eta_{L_R} L_R dW_7 \quad (21)$$

$$dH_S = \left[\pi_H - \frac{\sigma_4 H_S T_I}{N_T} - \frac{\sigma_5 H_S L_I}{N_L} - \frac{\sigma_6 H_S H_I}{N_H} - \mu_H H_S + \omega H_R\right] dt + \eta_{H_S} H_S dW_8 \quad (22)$$

$$dH_E = \left[\frac{\sigma_4 H_S T_I}{N_T} + \frac{\sigma_5 H_S L_I}{N_L} + \frac{\sigma_6 H_S H_I}{N_H} - (e_H + \mu_H) H_E\right] + \eta_{H_E} H_E dW_9 \quad (23)$$

$$dH_I = [e_H H_E - (\mu_H + \alpha_H + \delta_H) H_I] dt + \eta_{H_I} H_I dW_{10} \quad (24)$$

$$dH_R = [\alpha_H H_I - (\mu_H + \omega) H_R] dt + \eta_{H_R} H_R dW_{11} \quad (25)$$

Table 2 Description of Stochastic Noise Terms

Symbol	Description
$\eta_{T_S}, \eta_{T_E}, \eta_{T_I}$	Noise intensities associated with susceptible, exposed, and infectious tick compartments
W_1, W_2, W_3	Independent Wiener processes associated with the tick compartments
$\eta_{L_S}, \eta_{L_E}, \eta_{L_I}, \eta_{L_R}$	Noise intensities associated with susceptible, exposed, infectious, and recovered livestock compartments
W_4, W_5, W_6, W_7	Independent Wiener processes associated with the livestock compartments

Symbol	Description
$\eta_{H_S}, \eta_{H_E}, \eta_{H_I}, \eta_{H_R}$	Noise intensities associated with susceptible, exposed, infectious, and recovered human compartments
W_8, W_9, W_{10}, W_{11}	Independent Wiener processes associated with the human compartments

D. Numerical Approximation Using the Milstein Scheme

The stochastic CCHF model was numerically approximated using the Milstein scheme. Let

$$X(t) = (T_S, T_E, T_I, L_S, L_E, L_I, L_R, H_S, H_E, H_I, H_R)^T$$

denote the state vector. The stochastic model can be written in vector form as

$$dX(t) = f(X(t), t)dt + G\big(X(t)\big)dW(t), \quad (26)$$

where $f(X,t)$ is the drift vector, $W(t) = (W_1(t), W_2(t), \dots, W_{11}(t))^T$ is a vector of independent Wiener processes, and G(X) is the diffusion matrix. Environmental stochasticity was incorporated through multiplicative compartment-level perturbations. Consequently, the diffusion matrix is defined as

$$G(X) = diag(\eta_{T_S}T_S, \eta_{T_E}T_E, \eta_{T_I}T_I, \eta_{L_S}L_S, \eta_{L_E}L_E, \eta_{L_I}L_I, \eta_{L_R}L_R, \eta_{H_S}H_S, \eta_{H_E}H_E, \eta_{H_I}H_I, \eta_{H_R}H_R). \quad (27)$$

For each compartment,

$$g_i(X_i) = \eta_{X_i}X_i,$$

and therefore

$$\frac{\partial g_i}{\partial X_i} = \eta_{X_i}, \quad \text{and} \quad \frac{\partial g_i}{\partial X_j} = 0, i \neq j.$$

Hence, the Jacobian matrix of the diffusion coefficient is

$$J_{G(X)} = diag(\eta_{T_S}, \eta_{T_E}, \eta_{T_I}, \eta_{L_S}, \eta_{L_E}, \eta_{L_I}, \eta_{L_R}, \eta_{H_S}, \eta_{H_E}, \eta_{H_I}, \eta_{H_R}). \quad (28)$$

Because the diffusion matrix is diagonal and each compartment is driven by an independent Wiener process, all off-diagonal partial derivatives vanish. Consequently, the Jacobian matrix reduces to a diagonal matrix whose entries are the corresponding noise intensities. This considerably simplifies the Milstein correction term and eliminates the need for cross-derivative contributions.

For a time step Δt, the Wiener increments satisfy

$$\Delta W_{i,n} = W_i(t_{n+1}) - W_i(t_n) \sim N(0, \Delta t), \quad i = 1, \dots, 11. \quad (29)$$

The Milstein discretization of the stochastic CCHF model is therefore

$$X_{n+1} = X_n + f(X_n, t_n)\Delta t + G(X_n)\Delta W_n + \frac{1}{2} J_{G(X_n)}G(X_n)[(\Delta W_n)^2 - \Delta t] \quad (30)$$

The stochastic model was simulated over a period of 1095 days (three years). To quantify stochastic variability, multiple independent realizations were generated and the median trajectory together with the 5th and 95th percentile envelopes were computed for each compartment.

E. Positivity and Stability Analysis

The positivity of the stochastic system was analysed to ensure biological feasibility.

The model remains strictly positive for all time provided all initial conditions satisfy

$$T_S(0),\ T_E(0),\ T_I(0),\ L_S(0),\ L_E(0),\ L_I(0),\ L_R(0),\ H_S(0),\ H_E(0),\ H_I(0),\ H_R(0) > 0 \quad (31)$$

The disease-free equilibrium was analyzed using the Jacobian matrix.

The system is locally asymptotically stable whenever: (Van Den Driessche and Watmough, 2002)

$$R_0 < 1 \quad (32)$$

Detailed derivations are provided in the appendices.

F. Basic Reproduction Number

The basic reproduction number is defined as the expected number of secondary infections generated by one infected individual in a fully susceptible population (Van Den Driessche & Watmough, 2002).

Let

$$Y = (T_E, T_I, L_E, L_I, H_E, H_I)^T$$

denote the infected-state vector. By separating new infection terms from all other transition terms, the transmission matrix F and transition matrix V are constructed and evaluated at the disease-free equilibrium. The next-generation matrix is then given by $K = FV^{-1}$,

and the basic reproduction number is defined as the spectral radius

$$R_0 = \rho(FV^{-1}). \quad (33)$$

The detailed derivation of the matrices F and V and the computation of the spectral radius are provided in Appendix II. Analysis of the eigenvalues of the next-generation matrix shows that the transmission dynamics naturally decompose into two epidemiologically distinct pathways. The first pathway corresponds to the coupled tick–livestock transmission cycle, while the second pathway corresponds to direct human-to-human transmission. Consequently, the overall reproduction number is determined by the dominant transmission pathway and is given by

$$R_0 = max\{R_0^{TL}, R_0^H\} \quad (34)$$

Where

$$R_0^{(TL)} = \frac{A + \sqrt{A^2 + 4D}}{2} \quad (35)$$

And

$$R_0^{(H)} = \frac{\sigma_6 e_H}{(e_H + \mu_H)(\alpha_H + \mu_H + \delta_H)} \quad (36)$$

With $$A = \frac{\sigma_2 e_T}{\mu_T(\mu_T + e_T)} + \varepsilon \quad (37)$$

and

$$D = \frac{\sigma_1\sigma_3 e_T e_L}{\mu_T(\mu_T + e_T)(\alpha_L + \mu_L)(e_L + \mu_L)} \quad (38)$$

R_0^{TL}represents the reproduction potential generated by the tick–livestock transmission cycle, including both

horizontal transmission and vertical transmission in ticks. In contrast, R_0^H represents the reproduction potential associated with direct human-to-human transmission. Since sustained disease persistence can occur through either pathway, the overall threshold is determined by the larger of these two quantities. The disease-free equilibrium is stable when $R_0 < 1$ and unstable when $R_0 > 1$ (Van Den Driessche & Watmough, 2002)

III. MATERIALS AND METHOD

A. Study Area and Spatial Data

The study was conducted in Uganda using administrative district boundaries at the ADM2 level. District-level spatial units were used to evaluate geographically varying transmission potential and generate district-based risk maps. This spatial scale was selected because it provides sufficient geographic detail while remaining consistent with available climate and epidemiological datasets.

B. Climate Data Sources and Processing

Daily climatic variables were obtained primarily from ERA5-Land reanalysis datasets (Muñoz-Sabater *et al.*, 2021; Soci *et al.*, 2024). Temperature and relative humidity were extracted and used to compute vapor pressure deficit (VPD), which served as a key climate-dependent driver in the tick lifecycle model. CHIRPS precipitation data were used as supporting environmental reference where relevant (Funk *et al.*, 2015). These climatic variables were processed at district level and linked to spatial units for model parameterization.

C. Tick Lifecycle Parameterization

Climate-dependent tick lifecycle functions were parameterized using published ecological relationships (Randolph and Rogers, 2007; Estrada-Peña, Martínez Avilés and Muñoz Reoyo, 2011; Ogden, Mechai and Margos, 2013). Key biological and climate-dependent parameters were adapted from published *Hyalomma* ecological studies as describe in table 3.

Table 3 Key biological and climate-dependent parameters incorporated into the tick lifecycle model

Parameter	Description	Functional form / Value	Reference
b_T	Oviposition rate (eggs per female)	**6**,500 eggs per female (mean from 100 engorged females weighed in laboratory)	Estrada-Peña et al. (2011)
$\mu_T(T, VPD)$	Adult tick mortality rate (day⁻¹)	$M_a = 14.3 + 0.792T - 0.14VPD$(% day⁻¹); $\mu_T = M_a/100$; equivalent in kPa: $M_a = 14.3 + 0.792T - 1.4 \cdot VPD$	Estrada-Peña et al. (2011
$\mu_e(T, VPD)$, $\mu_l(T, VPD)$, $\mu_n(T, VPD)$	Egg, larval, and nymph stage mortality rates (day⁻¹)	$M_e = 108.325 - 3.848T + 1.414VPD$ (cumulative % over T_i); $M_l = 16.1 + 0.814T - 0.21VD$ (% day⁻¹); $M_n = 51.4786 + 1.525T - 0.22VPD$(cumulative % over$T_m$); daily rates: $\mu_E = M_e/(100 \cdot T_i)$, $\mu_l = M_l/100$, $\mu_n = M_n/(100 \cdot T_m)$	Estrada-Peña et al. (2011)
d_e, d_l, d_n	Egg, larval, and nymph developmental durations (days)	$dk(T) = a_k/(T - T_{0k})$for T > T_{0k}; T₀ = 7 °C for all stages; a_e= 130, a_l= 160, a_n= 140 (degree-day constants); ranges: $d_e \in$ [10, 30], $d_l \in$ [20, 60], $d_n \in$ [15, 40]	Randolph & Rogers (2007); Estrada-Peña et al. (2011)
f(T)	Temperature-dependent development rate (day⁻¹)	$f(T) = r_max \cdot (T - T_min)(T_max - T)^{1/2}$; $T_{min} = 7°C, T_{max} = 40°C, T_{opt} = 28°C, r_{max} = 0.10day^{-1}$	Brière et al. (1999); Estrada-Peña et al. (2011)
s(T, VPD)	Climate-dependent survival probability (dimensionless)	$s(T, VPD) = s_T(T) \cdot s_V(VPD)$; $s_T = exp(-\alpha_T \cdot (T - T_{(opt)})^2)$, α_T= 0.003 °C⁻²; s_V= $exp(-\alpha_V \cdot$ VPD), α_V= 0.15 kPa⁻¹; optimal temperature $T_{(opt)} = 28°C$	Estrada-Peña et al. (2011); Randolph & Rogers (2007)

The temperature-dependent development rate f(T) follows the Brière function (Brière et al., 1999), with parameters $T_{min} = 7°C$and $T_{max} = 40°C$ calibrated to the developmental thresholds reported for *Hyalomma marginatum* (Estrada-Peña, Martínez Avilés and Muñoz Reoyo, 2011). Tick mortality parameters were taken directly from the linear regression equations fitted by Estrada-Peña

et al. (2011). Survival probability s(T, VPD) is expressed as the product of a Gaussian temperature response and a negative exponential vapor pressure deficit response, adapted from the empirical relationships in Estrada-Peña et al. (2011) and the desiccation principles discussed in Randolph and Rogers (2007), and captures the unimodal dependence of tick activity on temperature alongside the monotonic decline in survival under increasing atmospheric dryness.

These functional forms were evaluated at each daily time step using ERA5-Land temperature and computed vapor pressure deficit for each district, and the resulting time-varying tick parameters were passed to the Milstein integration scheme to drive climate-dependent tick dynamics over the simulation horizon.

D. Numerical Simulation Procedure

The stochastic model was simulated numerically over a period of 1095 days (three years) to capture multi-seasonal tick generation cycles and long-term disease persistence behaviour. The Milstein scheme was applied with a fixed time step of $\Delta t = 0.5$ days. Initial conditions were set to represent a low-level endemic state at the start of the simulation, consistent with the epidemiological context of CCHF in Uganda. The numerical values used in all simulations are reported in Table 4. These values were selected on the basis of the analytical endemic equilibrium derived from the model equations, ensuring that the simulation begins near a biologically plausible endemic state rather than an arbitrary starting point.

Table 4 numerical values used in all simulations

Variables	**Initial value**
Susceptible ticks $(T_S(0))$	5,188
Exposed ticks $(T_E(0))$	53
Infectious ticks $(T_I(0))$	1,062
Susceptible livestock $(L_S(0))$	988
Exposed livestock $(L_E(0))$	329
Infectious livestock $(L_I(0))$	631
Recovered livestock $(L_R(0))$	3,680
Susceptible humans $(H_S(0))$	1,256
Exposed humans $(H_E(0))$	52
Infectious humans $(H_I(0))$	23
Recovered humans $(H_R(0))$	191

The simulation outputs included, host and vector trajectories, prevalence indicators, incidence, seasonal variation.

These outputs were used to evaluate temporal dynamics under stochastic environmental forcing.

A. Milstein Convergence Verification

To assess the numerical reliability of the stochastic simulations, a step-size sensitivity analysis was performed by comparing the Milstein scheme with the Euler–Maruyama method. Simulations were conducted using decreasing time-step sizes ($\Delta t = 0.10$, 0.05, 0.025, and 0.0125), and the relative numerical errors were computed with respect to a high-resolution reference solution.

Figure 2 illustrates the relationship between the relative error and the time-step size for both numerical schemes. As expected, the numerical error decreased as the time step was reduced. The estimated convergence slopes were approximately 1.401 for the Milstein scheme and 0.613 for the Euler–Maruyama scheme.

These results are consistent with the theoretical strong convergence orders of 1.0 for the Milstein method and 0.5 for the Euler–Maruyama method. Furthermore, the Milstein scheme consistently produced lower numerical errors than Euler–Maruyama for all tested time-step sizes. This confirms the suitability of the Milstein approximation for the stochastic CCHF model and supports the reliability of the numerical simulations reported in this study.

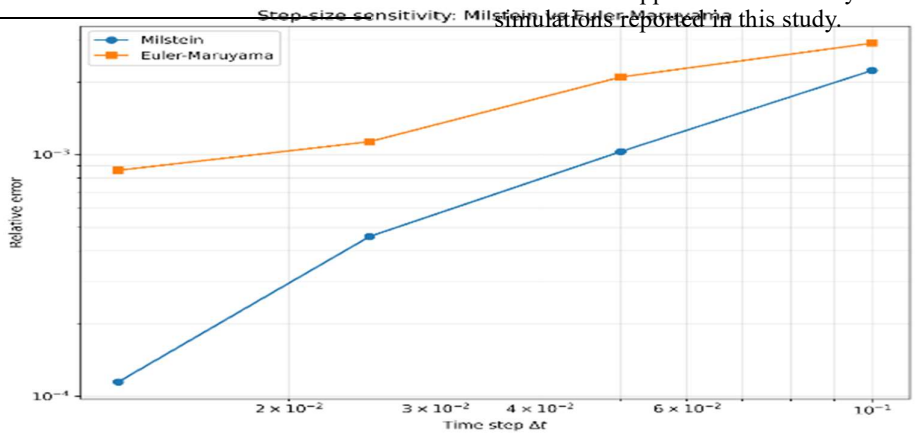

Figure 2 Step-size sensitivity analysis and convergence comparison between the Milstein and Euler–Maruyama schemes. The Milstein method exhibits lower numerical errors and a higher convergence rate, consistent with its theoretical strong order of convergence.

The computational cost of the Milstein scheme for the eleven-dimensional stochastic system was evaluated on a standard desktop computer (Intel Core i7, 16 GB RAM) running Python 3.11. Each individual stochastic realisation

over the 1095-day horizon with $\Delta t = 0.5$ days required approximately 0.8 seconds of wall-clock time. Generating the full ensemble of 300 independent realisations required approximately four minutes per scenario, and the complete analysis including both parameter scenarios, sensitivity analysis, and spatial risk mapping was completed within approximately fifteen minutes. These runtimes confirm that the Milstein implementation is computationally feasible for the purpose of ensemble-based uncertainty quantification and scenario analysis. The time step $\Delta t = 0.5$ days was selected on the basis of the convergence analysis presented in Section III.F, which demonstrated that this value provides a satisfactory balance between numerical accuracy and computational efficiency for the present model.

B. Spatial Risk Mapping and Preliminary Validation

Climate-driven transmission potential was estimated at district level using $R_0(s)$, where s denotes geographic location. District values were mapped using R tools to produce spatial risk maps. For preliminary validation, districts with reported CCHF occurrence were compared qualitatively with model-based classifications (Omoga *et al.*, 2023; Balinandi *et al.*, 2024; Zalwango *et al.*, 2024). This approach provided a first-level comparison between observed occurrence and predicted climate-driven transmission risk. To complement the qualitative comparison, a simple binary agreement score was calculated as the ratio between matching district classifications and the total number of districts compared. This metric provides an interpretable first-level measure of consistency between reported CCHF occurrence and model-predicted spatial risk.

C. Spatial and Climatic Considerations

Although the mathematical model does not explicitly include spatial diffusion or host mobility, spatial heterogeneity is incorporated through climate-driven parameterization. Environmental variables at district level modify tick recruitment, mortality, development and transmission coefficients (Estrada-Peña, Martínez Avilés and Muñoz Reoyo, 2011; Ogden, Mechai and Margos, 2013). This indirect spatialization allows computation of district-specific epidemiological indicators while remaining computationally efficient. The resulting framework enables climate-informed mapping of transmission potential and identification of high-risk districts where environmental conditions favor sustained CCHF transmission.

D. Uncertainty and Sensitivity Analysis

To quantify the influence of parameter uncertainty on the basic reproduction number, a global sensitivity analysis was performed using Latin Hypercube Sampling (LHS) coupled with Partial Rank Correlation Coefficients (PRCCs). Parameter values were sampled from the biologically plausible ranges reported in Table 5. A total of 1000 parameter sets were generated using LHS and propagated through the analytical expression of the basic reproduction number (R_0). PRCC values were subsequently computed to assess the relative influence of each parameter on (R_0). Parameters with large positive PRCC values increase disease transmission, whereas parameters with large negative PRCC values reduce transmission.

Table 5 Parameters and ranges used in the LHS sensitivity analysis

Parameter	Range	Unit	Reference
π_l	[0.5, 1.5]	Livestock/Time	Mpeshe et al. (2011)
π_h	[0.5, 1.5]	Human/Time	Mpeshe et al. (2011)
π_t	[0.5, 3.5]	Tick/Time	Sutton et al. (2012)
μ_l	[1/3600, 1/360]	1/Time	Mpeshe et al. (2011)
μ_h	[1/(365×60), 1/(365×40)]	1/Time	Mpeshe et al. (2011)
μ_t	[1/365, 1/30]	1/Time	Mpeshe et al. (2011)
e_t	[1/3, 1]	1/Time	Matser et al. (2009); Shayan et al. (2015)
e_l	[1/5, 1/3]	1/Time	Matser et al. (2009)
e_h	[1/9, 1]	1/Time	Shayan et al. (2015)
ε	[0.14, 0.20]	Number	Matser et al. (2009)
α_l	[1/21, 1/14]	1/Time	Hoch et al. (2018)

Parameter	Range	Unit	Reference
α_h	[1/21, 1/15]	1/Time	Shayan et al. (2015)
σ_1	[0.11, 0.33]	Number	Matser et al. (2009)
σ_2	[0.01, 0.04]	Number	Matser et al. (2009)
σ_3	[0.13, 0.71]	Number	Matser et al. (2009)
σ_4	[0.25, 0.375]	Number	Kriesel et al. (2009)
σ_5	[0.001, 0.002]	Number	Mpeshe et al. (2011)
σ_6	[0.26, 0.75]	Number	Mondal et al. (2017)
δ_h	[0.3, 0.8]	1/Time	Schuster et al. (2016); Shayan et al. (2015)

IV. RESULTS AND DISCUSSION

Numerical simulations were performed using the Milstein stochastic scheme to evaluate the behaviour of the proposed climate-driven CCHF transmission model under environmental variability (Kloeden and Platen, 1992). A total of 300 independent stochastic realisations were generated over a three-year (1095-day) simulation horizon to characterise the uncertainty induced by multiplicative environmental noise. Two parameter scenarios were examined: an endemic scenario representing conditions consistent with observed CCHF persistence in Uganda ($R_0 = 2.42$), and a sub-threshold scenario representing unfavourable environmental conditions under which disease extinction occurs ($R_0 = 0.70$). Both scenarios were initiated from identical starting conditions to ensure that observed differences in long-term behaviour reflect parameter-driven dynamics rather than differences in initial infection levels.

A. Endemic Scenario: Seasonal Persistence and Stochastic Variability

Under the endemic parameterisation ($R_0 = 2.42$), the deterministic model converges to a stable endemic regime characterised by sustained seasonal oscillations across all compartments. Figure 3(a) presents the temporal evolution of the total infectious burden $Z(t) = T_I + L_I + H_I$ over the three-year simulation period. The deterministic trajectory exhibits a pronounced bimodal seasonal pattern consistent with Uganda's two rainfall seasons, with Z(t) oscillating between a trough of approximately 1,320 and a peak of approximately 2,993 infectious individuals across the tick, livestock, and human populations combined.

The stochastic realisations generate substantial variability around the deterministic trajectory. The 5th–95th percentile interval spans from approximately 1,180 to 2,501 at the end of the simulation horizon (day 1,095), confirming that environmental stochasticity introduces considerable uncertainty in disease burden predictions even when the long-term mean dynamics are well characterised. The stochastic median remains close to the deterministic trajectory throughout, consistent with the theoretical behaviour of multiplicative noise systems in which the median provides a robust central estimate (Mao, 2007). None of the 300 stochastic realisations reached the extinction threshold $Z(t) \leq 1$ over the three-year horizon, confirming that $R_0 > 1$ produces robust disease persistence even under environmental fluctuations.

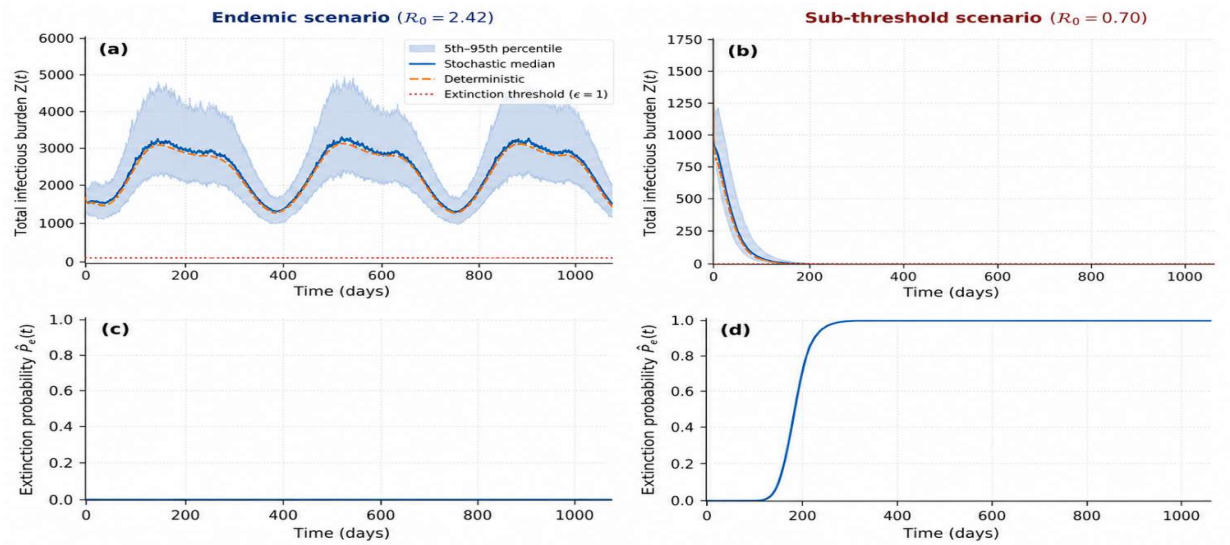

Figure 3 Total infectious burden $Z(t) = T_I + L_I + H_I$ over the three-year simulation horizon under (a) the endemic scenario and (b) the sub-threshold scenario. Lines show the deterministic trajectory and stochastic median; shaded bands show the 5th–95th percentile envelope across 300 stochastic realisations. (c)–(d) Corresponding empirical extinction probability over time for the endemic and sub-threshold scenarios, respectively.

Figure 4 presents the tick compartment dynamics. Susceptible ticks T_S exhibit pronounced bimodal seasonal oscillations driven by climate-dependent recruitment, ranging from a trough of approximately 1,500 to a peak of approximately 5,500 individuals. Exposed ticks T_E and infectious ticks T_I follow the same seasonal rhythm with a characteristic developmental lag, with infectious ticks peaking at approximately 2,375 individuals near day 897 and declining to a seasonal trough of approximately 713 near day 400. These oscillations directly reflect the influence of temperature and vapor pressure deficit on tick development and survival, incorporated through the climate-forcing function (Estrada-Peña, Martínez Avilés and Muñoz Reoyo, 2011; Ogden, Mechai and Margos, 2013). The stochastic uncertainty band on T_I is wide relative to the mean, indicating that tick infection prevalence is highly sensitive to environmental perturbations, with direct implications for the timing and intensity of spillover events to livestock and humans.

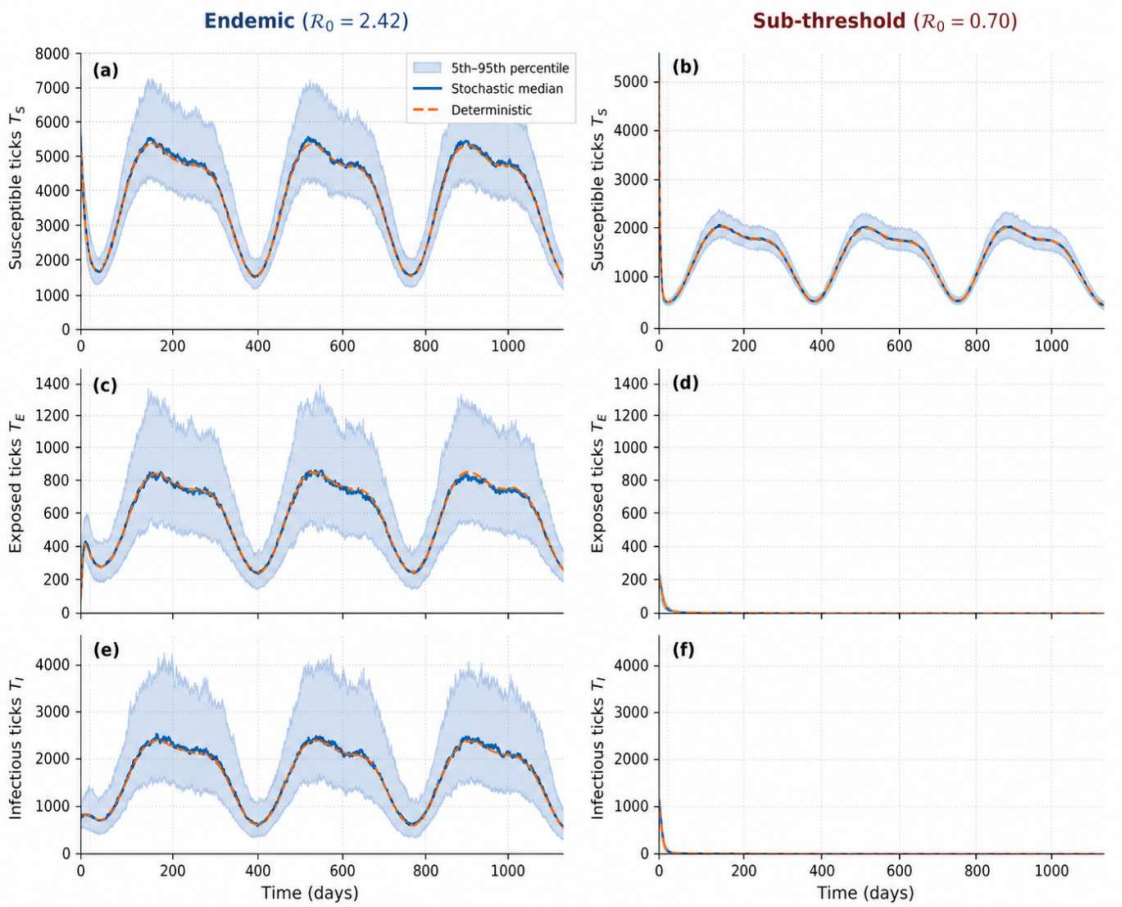

Figure 4 Tick compartment dynamics under the endemic and sub-threshold scenarios. (a)-(b) Susceptible ticks T_S;(c)-(d) Exposed ticks T_E; (e)-(f) Infectious ticksT_I. Shaded bands show the 5th-95th percentile envelope across 300 stochastic realisations.

Figure 5 presents the livestock compartment dynamics. Susceptible livestock L_S undergo a sharp initial decline from the starting value before settling into a low seasonal oscillation between approximately 450 and 700 individuals, reflecting the continuous depletion of the susceptible pool by sustained tick-to-livestock transmission pressure. Exposed livestock L_E stabilise at approximately 329 individuals, while infectious livestock L_I maintain an endemic level of approximately 597, confirming the role of livestock as the principal amplifying host in the CCHF transmission cycle. The recovered livestock compartment L_R is the largest among the infected classes, reflecting the predominantly subclinical nature of CCHF in ruminants and the accumulation of immune individuals over time (Bernard et al., 2022). The wide stochastic uncertainty band on L_I and L_R reflects the amplification of tick infection variability through the tick-to-livestock transmission pathway.

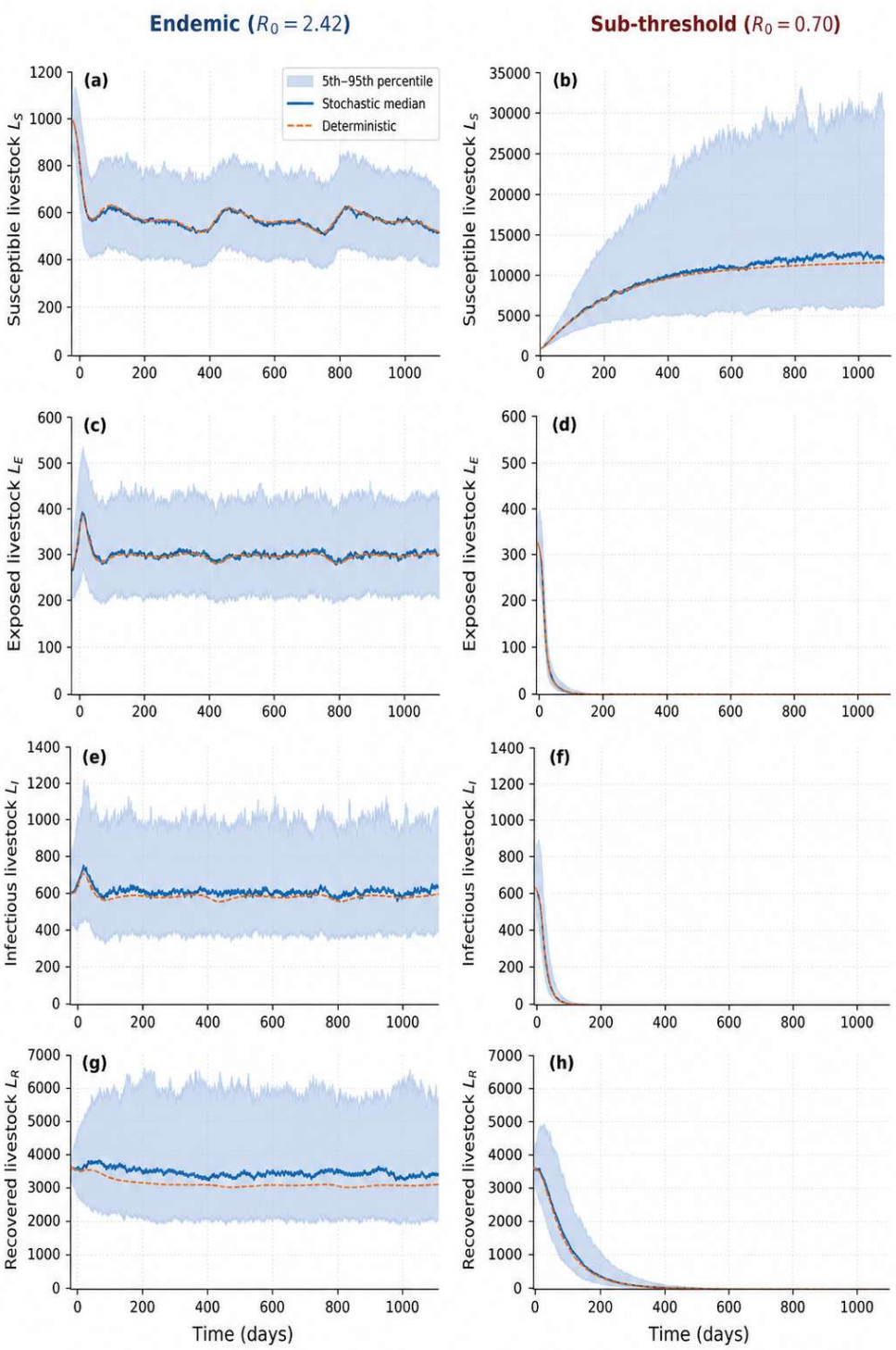

Figure 5 Livestock compartment dynamics under the endemic and sub-threshold scenarios. (a)-(b) Susceptible livestock L_S; (c)-(d) Exposed livestock L_E; (e)-(f) Infectious livestock L_I; (g)-(h) Recovered livestock L_R. Shaded bands show the 5th-95th percentile envelope across 300 stochastic realisations.

Figure 6 presents the human compartment dynamics. Susceptible humans H_S decline gradually from the initial value before stabilising near 850–950 individuals with modest seasonal fluctuation. Exposed humans H_E remain comparatively low throughout, reflecting the short incubation period before progression to the infectious class. Infectious humans H_I maintain a stable endemic level of approximately 27 cases, substantially lower than L_I, consistent with the spillover character of human CCHF infection and the lower probability of tick-to-human and livestock-to-human transmission incorporated through σ_4 and σ_5. The stochastic uncertainty on H_I spans approximately 15 to 55 cases throughout the simulation horizon, highlighting variability in human case burden that cannot be

captured by deterministic models alone. Recovered humans H_R accumulate progressively, indicating the development of population immunity over time. Taken together, the endemic compartment dynamics confirm that the proposed model reproduces biologically realistic CCHF transmission patterns, with the ordering $T_I \gg L_I \gg H_I$ reflecting the tick-reservoir, livestock-amplifier, human-spillover transmission hierarchy characteristic of CCHF epidemiology (Bhowmick et al., 2022).

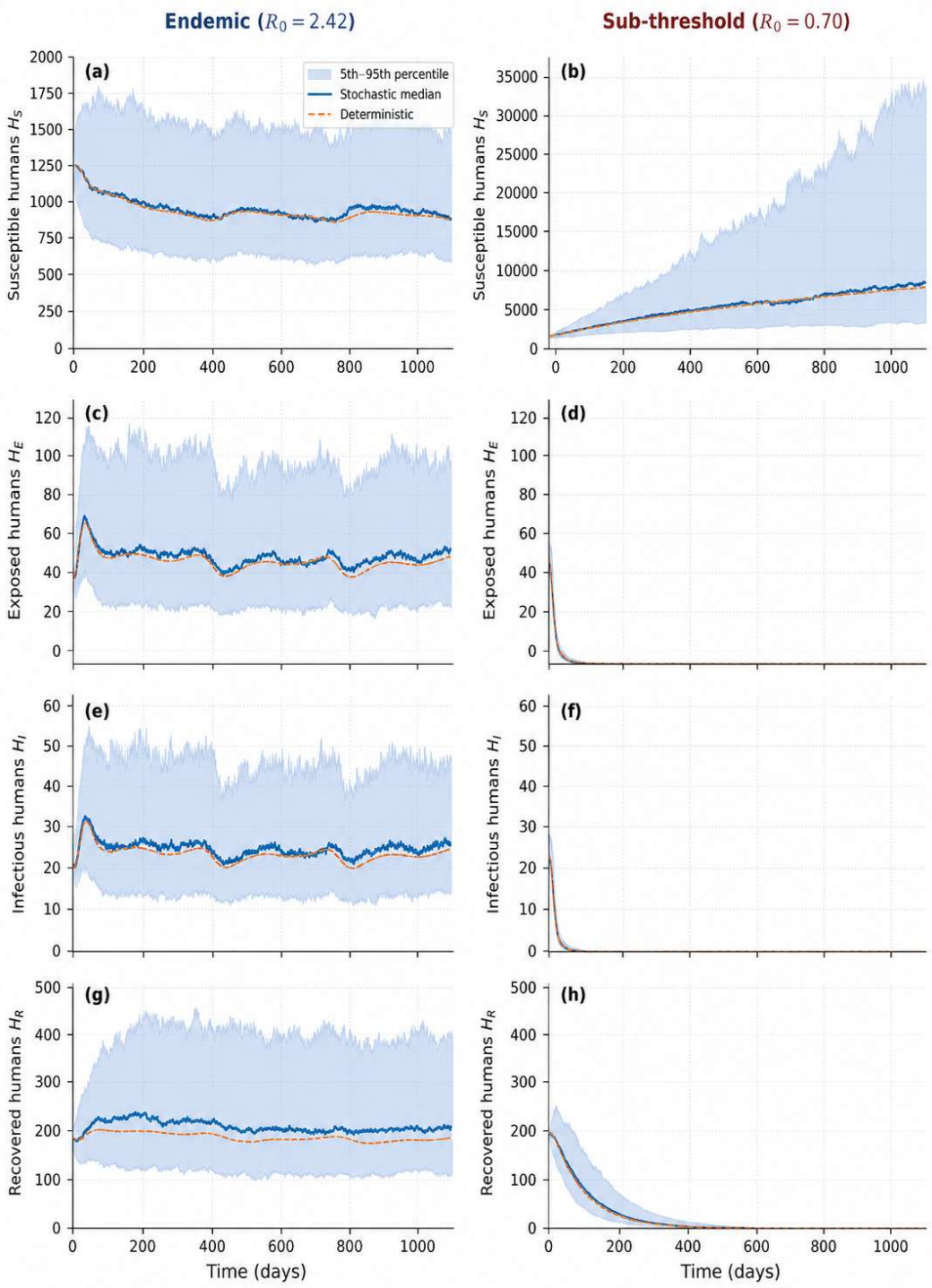

Figure 6 Human compartment dynamics under the endemic and sub-threshold scenarios. (a)-(b) Susceptible humans H_S; (c)-(d) Exposed humans H_E; (e)-(f) Infectious humans H_I; (g)-(h) Recovered humans H_R. Shaded bands show the 5th-95th percentile envelope across 300 stochastic realisations.

B. Sub-threshold Scenario: Disease Extinction Under Unfavourable Conditions

To numerically verify the extinction conditions derived analytically in Appendix III, a sub-threshold parameter scenario was examined under conditions of high environmental stress on tick populations. Under these conditions the basic reproduction number falls to $R_0 = 0.70$, placing the system below the epidemic threshold. The sub-threshold scenario was initiated from identical starting conditions to the endemic scenario, so that observed differences in outcome are attributable solely to the parameter change. Figure 3(b) presents Z(t) under the sub-threshold scenario. The deterministic trajectory declines monotonically from the initial value of 1,716 infectious individuals, crossing the extinction threshold Z(t) = 1 within approximately 150 days and converging to zero thereafter. The stochastic realisations follow the same declining trajectory, with the Monte Carlo median closely tracking the deterministic solution. In contrast to the endemic scenario, the stochastic uncertainty band narrows progressively as infection levels decline, reflecting reduced multiplicative noise contributions as compartment sizes approach zero.

Figures 4(b), (d), and (f); 5(b), (d), (f), and (h); and 6(b), (d), (f), and (h) present the tick, livestock, and human compartments under the sub-threshold scenario. Exposed and infectious ticks both decay rapidly to near zero within the first 100 days, removing the primary source of infection pressure on livestock and humans. Exposed and infectious livestock follow with a short delay, declining to extinction by approximately day 200; exposed and infectious humans extinguish within approximately 100 days, consistent with the low human exposure rates incorporated through σ_4 and σ_5. Recovered livestock and recovered humans exhibit characteristic hump-and-decay profiles, rising initially as previously exposed individuals recover and then declining as no new infections replenish the classes.

Notably, the susceptible compartments behave very differently from the infected classes under sub-threshold conditions. With infection pressure collapsing, susceptible ticks, livestock, and humans are no longer continuously depleted, and each compartment grows toward its disease-free demographic equilibrium. Susceptible livestock and susceptible humans in particular do not reach this new equilibrium within the three-year simulation horizon, still rising at day 1,095, reflecting the comparatively slow demographic turnover of these host populations relative to the much faster epidemic fade-out timescale of approximately 200–300 days.

Figure 7 presents the empirical extinction probability estimated from the 300 stochastic realisations, with extinction defined as $Z(t) = T_I(t) + L_I(t) + H_I(t) \leq 1$. The extinction probability remains negligible during the first 100 days, while the initial infectious burden is still substantial. A rapid transition follows, with the extinction probability reaching 50% at approximately day 174, 90% at approximately day 220, and 99% at approximately day 274. By the end of the simulation horizon, all 300 stochastic realisations had reached the extinction threshold, yielding an empirical extinction probability of 100%. This constitutes direct numerical confirmation of the analytical extinction condition established in Appendix III: when $R_0 < 1$, environmental stochasticity accelerates disease fade-out rather than sustaining infection above the extinction threshold.

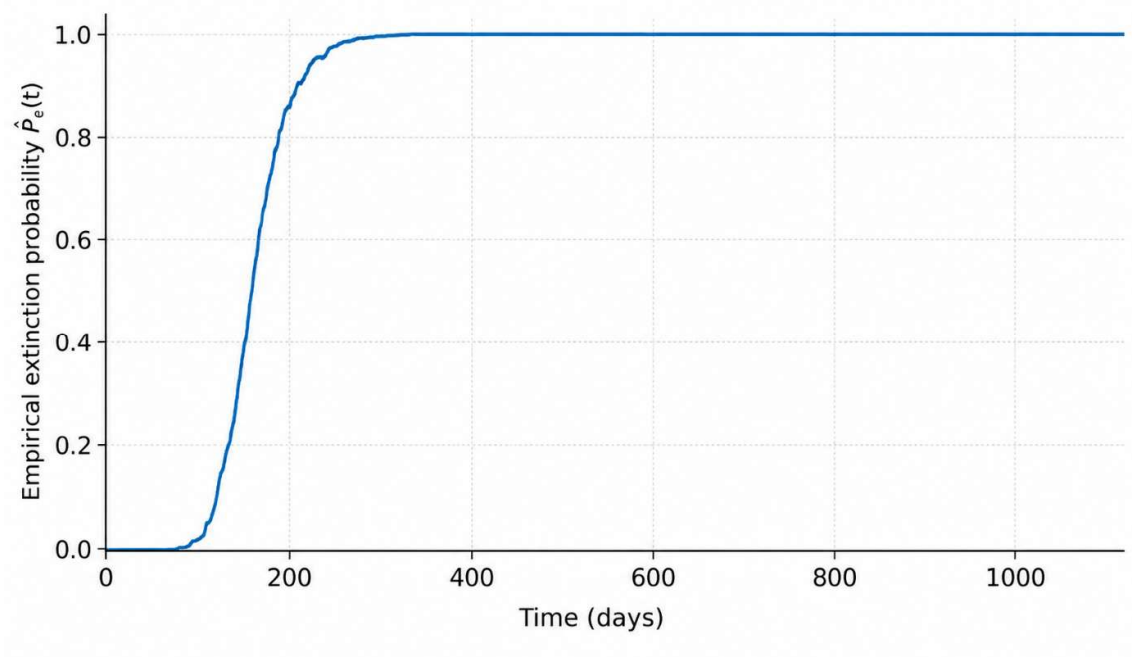

Figure 7 Empirical extinction probability over time for the sub-threshold scenario, estimated from 300 stochastic realisations.

C. Comparison of Scenarios and Implications for Disease Control

The contrast between the two scenarios in Figure 3 illustrates the critical role of R_0 as a threshold parameter governing long-term CCHF dynamics. Under endemic conditions (R_0 = 2.42), sustained seasonal transmission persists across all three host populations over the full three-year horizon, with environmental stochasticity producing substantial but bounded variability around the endemic regime. Under sub-threshold conditions (R_0 = 0.70), the identical initial outbreak declines to extinction within approximately 200–300 days regardless of the stochastic realisation, with disease fade-out occurring faster in the stochastic system than the deterministic trajectory alone would suggest, due to the amplification of extinction events by environmental noise.

These findings carry direct implications for CCHF surveillance and control in Uganda. The endemic scenario parameters, which incorporate realistic Ugandan tick biology and transmission rates, produce persistent year-round human case burdens with pronounced seasonal peaks corresponding to Uganda's bimodal rainfall pattern. Interventions that sufficiently reduce tick survival or eliminate vertical transmission pathways to bring R_0 below unity would, according to these results, drive disease extinction within approximately six to nine months even when initiated during active transmission. These targets may be achievable through sustained acaricide application and livestock management practices timed to the dry seasons, which correspond to minimum tick activity and lowest seasonal values of the climate-forcing function (Estrada-Peña, Martínez Avilés and Muñoz Reoyo, 2011; Ogden, Mechai and Margos, 2013).

The stochastic framework developed here captures variability in outbreak magnitude that deterministic models cannot reproduce. As demonstrated by the wide 5th–95th percentile intervals in Figures 4–6, the human infectious burden H_I can vary by a factor of approximately three to four around the deterministic prediction under realistic environmental noise. This has direct implications for health system preparedness: surveillance systems calibrated solely to the deterministic endemic equilibrium would systematically underestimate peak outbreak risk during periods of stochastic amplification, and overestimate baseline case burden during unfavourable periods. Integration of stochastic uncertainty bounds into CCHF surveillance thresholds would therefore improve the sensitivity and specificity of early warning systems in Uganda and similar endemic settings (Zalwango et al., 2024; Balinandi et al., 2024).

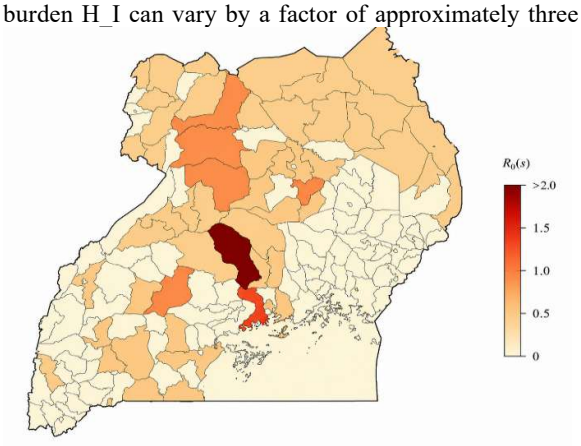

Figure 8 Spatial distribution of the climate-driven basic reproduction number $R_0(s)$ across Uganda at ADM2 district level. Districts with $R_0(s) > 1$ represent areas where environmental conditions may support sustained CCHF transmission.

E. Spatial Uncertainty Analysis

To quantify uncertainty in the spatial transmission risk estimates, a Monte Carlo uncertainty propagation analysis was performed for each district. District-level reproduction numbers were repeatedly sampled within the prescribed uncertainty bounds and the probability that the climate-driven reproduction number exceeded the epidemic threshold was estimated as $P(R_0(s) > 1)$.

D. Spatial Distribution of Climate-Driven Transmission Risk.

Figure 8 presents the spatial distribution of climate-driven transmission potential. The results reveal substantial spatial heterogeneity. Several districts exhibit values of $R_0(s) > 1$, indicating environmental conditions favorable for sustained transmission. Higher-risk districts are concentrated primarily in central Uganda, with moderate transmission potential extending into some neighbouring southern districts, whereas lower transmission potential is observed across much of northern and northeastern regions. These spatial differences reflect the influence of localized climatic conditions on tick survival, development, and host-contact processes.

The spatial analysis demonstrates pronounced heterogeneity in district-level transmission potential. Similar spatial variability has been reported in previous epidemiological studies and is closely associated with climatic suitability, livestock distribution, and vector ecology (Omoga *et al.*, 2023; Balinandi *et al.*, 2024; Zalwango *et al.*, 2024). The resulting spatial map provides a climate-informed representation of district-level CCHF transmission risk and identifies priority areas for surveillance and targeted intervention.

Figure 9 presents the resulting uncertainty map. Districts were classified according to the probability of sustaining transmission under parameter uncertainty. Several districts located in central and northwestern Uganda exhibited very high probabilities of satisfying ($R_0(s) > 1$), indicating that favorable transmission conditions remained robust across uncertainty realizations. In contrast, many districts in eastern and southwestern Uganda displayed lower probabilities, suggesting weaker support for sustained transmission under uncertain conditions.

Compared with the deterministic spatial map, the probabilistic representation provides additional information regarding the confidence associated with district-level risk estimates. Districts characterized by high values of $P(R_0(s) > 1)$ represent areas where transmission suitability remains consistently elevated despite uncertainty in model parameters and climatic inputs. These areas may therefore constitute priority locations for surveillance and targeted intervention.

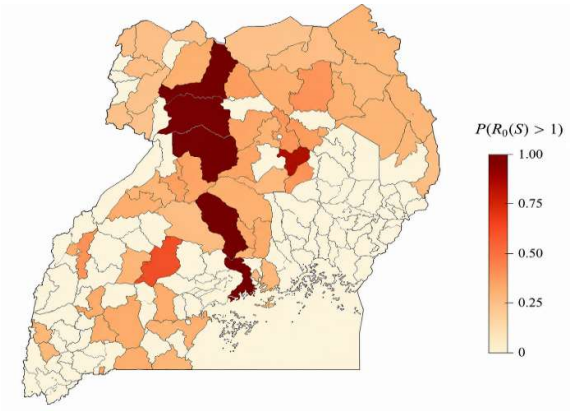

Figure 9 District-level probability that the climate-driven reproduction number exceeds the epidemic threshold, $P(R_0(s) > 1)$, obtained through Monte Carlo uncertainty propagation. Darker colors indicate districts where sustained transmission remains likely across a larger proportion of uncertainty realizations.

F. Spatial Validation of Climate-Driven Risk Predictions

To evaluate the consistency between model predictions and observed CCHF occurrence, reported outbreak records were compared with districts classified as high-risk according to the climate-driven reproduction number. Districts were classified as high-risk when their climate-driven reproduction number exceeded 1 ($R_0(s) > 1$). A binary agreement analysis was performed using a confusion matrix comparing observed outbreak occurrence and model-predicted risk classification. The resulting validation metrics yielded an overall agreement score (accuracy) of 79.6%, with a sensitivity of 71.1% and a specificity of 79.9%.

Several districts were classified as high-risk despite the absence of reported outbreaks. These apparent false positives should not necessarily be interpreted as model failures. The climatic suitability represented by (R_0) reflects the potential for sustained transmission if the virus is introduced, whereas observed outbreaks additionally depend on surveillance intensity, pathogen introduction events, livestock movement, human exposure patterns, and reporting capacity. Consequently, districts predicted as high-risk but lacking reported outbreaks may represent areas of latent transmission potential that warrant enhanced surveillance and monitoring.

While a full retrospective temporal calibration against specific outbreak years was not possible due to the absence of publicly available weekly or monthly CCHF case-count time series for Uganda, the spatial validation provides a meaningful consistency check for the model's predictions. As a specific example, the Rakai district outbreak of 2022, one of the most clearly documented recent CCHF events in Uganda (Balinandi et al., 2024; Zalwango et al., 2024) corresponds to a district classified as high-risk ($R_0(s) > 1$) in the climate-driven spatial analysis, consistent with the model's prediction that environmental conditions in Rakai are conducive to sustained CCHF transmission. Similarly, the Nakaseke and Kyankwanzi outbreaks of 2018 and 2024, respectively, are located within districts identified as high-risk in the spatial risk map. These qualitative agreements provide preliminary support for the spatial risk classification produced by the model. Full temporal validation against retrospective case incidence data would require systematic surveillance records at sub-annual resolution, which currently represent a critical data gap for CCHF in Uganda and are identified as a priority for future research.

G. Global Sensitivity Analysis of R_0

Figure 10 presents the PRCC values obtained from the global sensitivity analysis of the basic reproduction number R_0.

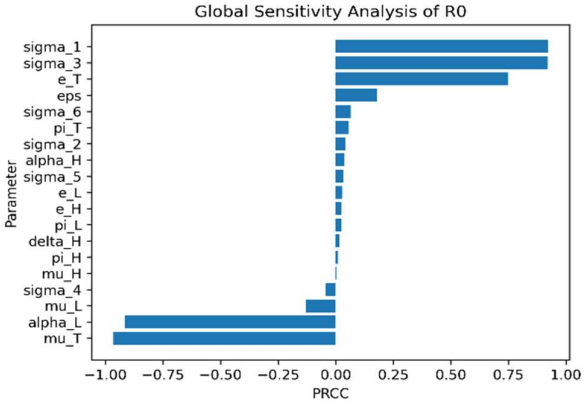

Figure 10 Global sensitivity analysis of the basic reproduction number R_0 based on Latin Hypercube Sampling (1000 samples) and Partial Rank Correlation Coefficients (PRCCs)

The global sensitivity analysis identified tick mortality (μ_T) as the most influential parameter affecting the basic reproduction number, with a PRCC value of -0.946. This strong negative association indicates that increasing tick mortality substantially reduces disease transmission. Among the transmission parameters, tick-to-livestock transmission (σ_3) and livestock-to-tick transmission (σ_1) exhibited the strongest positive influence on R_0, with PRCC values of 0.866 and 0.755, respectively. These findings highlight the dominant role of the tick–livestock transmission cycle in sustaining CCHF transmission.

The livestock recovery rate (α_L) showed a considerable negative effect (−0.438), indicating that shortening the infectious period of livestock can meaningfully reduce transmission. Tick-to-tick transmission (σ_2) had a modest positive influence (0.202). The vertical transmission fraction (ε) showed a small positive effect (0.023), consistent with its role as an additive, dimensionless contribution to the tick-to-tick component of R₀ under the corrected formulation. The remaining parameters including σ_4, $\sigma_5, \sigma_6, e_H, e_L, \alpha_H, \delta_H$, and the recruitment terms π_L, π_H, π_T displayed weak effects on R₀ (|PRCC| < 0.05), indicating that overall transmission dynamics are primarily governed by the tick–livestock cycle rather than direct human-to-human transmission or demographic turnover.

H. Climate-Driven Tick Lifecycle Dynamics

Climate-dependent tick lifecycle functions were incorporated to examine how environmental forcing influences vector dynamics and transmission potential. Figure 11 presents the climatic forcing profiles used in the simulations. Temperature exhibits moderate seasonal variability throughout the year, whereas vapor pressure deficit displays stronger fluctuations associated with atmospheric dryness.

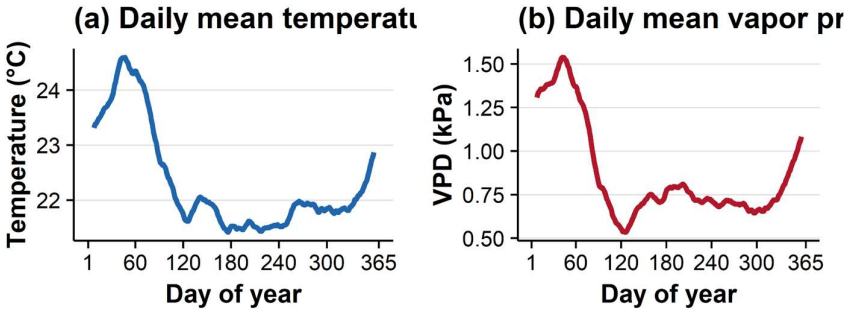

Figure 11 Daily climatic forcing used in the model: (a) temperature and (b) vapor pressure deficit. These variables regulate climate-sensitive tick development, mortality, and survival functions.

Figure 12 illustrates how these climatic variables influence tick lifecycle parameters. Warmer periods shorten development durations and accelerate transitions between tick stages. Conversely, elevated vapor pressure deficit increases desiccation stress and reduces survival probabilities. These nonlinear environmental responses introduce seasonal variability into vector abundance and directly influence the force of infection exerted on livestock and human populations. An important contribution of the present study is the integration of temperature and vapor pressure deficit dependent tick lifecycle functions into a stochastic epidemiological framework. This coupling provides a mechanistic representation of how environmental forcing modifies vector abundance and infection pressure over time, thereby strengthening the connection between ecological vector dynamics and epidemiological transmission processes (Estrada-Peña, Martínez Avilés and Muñoz Reoyo, 2011; Ogden, Mechai and Margos, 2013).

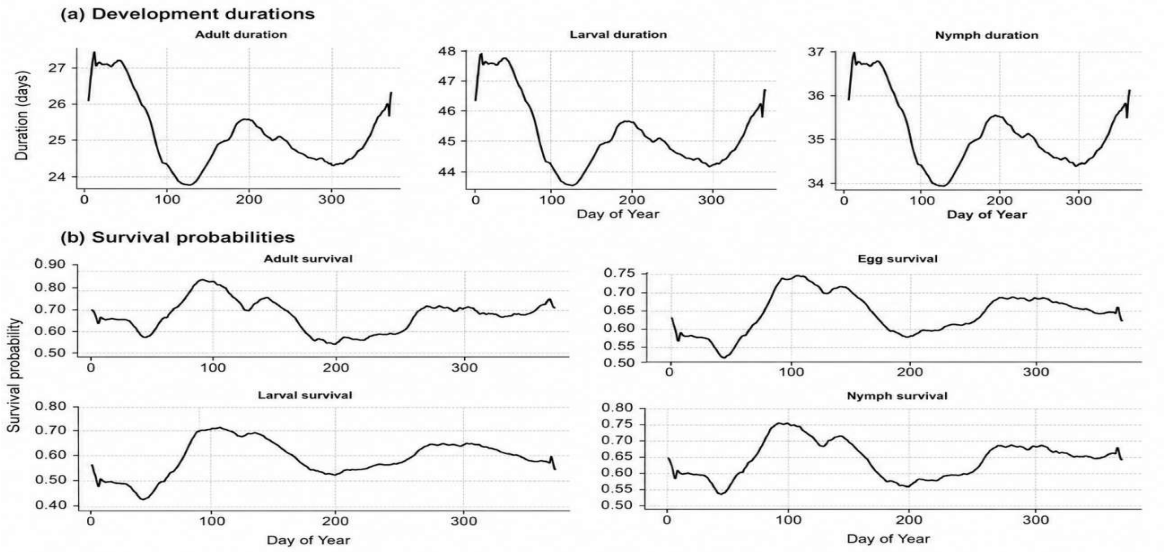

Figure 12 Climate-driven tick lifecycle parameters under realistic climatic forcing: (a) temperature-dependent development and transition durations and (b) stage-specific survival probabilities regulated by temperature and vapor pressure deficit.

Overall, the results indicate that temperature and vapor pressure deficit jointly regulate the timing and intensity of vector-driven transmission. Favourable climatic periods promote faster development and improved survival, whereas dry conditions suppress vector persistence. These climate-induced variations propagate through the epidemiological system and generate pronounced seasonal fluctuations in CCHF transmission potential across Uganda. From a broader epidemiological perspective, the findings demonstrate that environmental variability strongly influences CCHF transmission, and that climate-informed stochastic modelling provides a useful framework for understanding disease dynamics, identifying priority surveillance areas, and supporting environmentally targeted intervention planning.

I. Threshold-Based Control Implications

The analytical and numerical results of this study provide a direct basis for threshold-informed CCHF control in Uganda. The basic reproduction number R_0 serves as the primary decision variable: any combination of interventions that reduces R_0 below unity is sufficient to drive disease extinction, as demonstrated by the sub-threshold simulation scenario in Section IV.A. The sensitivity analysis (Section III.G) identifies tick mortality $\mu_T$as the parameter with the strongest negative influence on R_0 (PRCC = −0.946), followed by tick-to-livestock transmission σ_3 (PRCC = 0.866) and livestock-to-tick transmission σ_1 (PRCC = 0.755). These results suggest that acaricide-based tick control, which simultaneously increases effective tick mortality and reduces tick-host contact rates, represents the most efficient single-intervention lever for reducing R_0.

The spatial risk map (Section IV.C) identifies districts where $R_0(s) > 1$ under current climatic conditions. These districts represent priority targets for interventions. A district-level decision rule derived from the model is: deploy enhanced acaricide campaigns and livestock surveillance in districts where $P(R_0(s) > 1) \geq 0.70$ (as estimated by the Monte Carlo uncertainty analysis in Section IV.D), and maintain baseline passive surveillance in districts where $P(R_0(s) > 1) < 0.30$. Districts in the intermediate range ($0.30 \leq P(R_0(s) > 1) < 0.70$) represent areas of uncertain transmission suitability where targeted active surveillance and seasonal tick monitoring would be most cost-effective. The seasonal component of the model further suggests that interventions timed to the onset of the primary Uganda rainfall season (March–May), when tick recruitment peaks and R_0 is at its seasonal maximum, would produce the greatest reduction in peak transmission intensity.

From a resource allocation perspective, the spatial uncertainty analysis provides a practical basis for prioritising limited public health budgets. Of Uganda's 146 ADM2 districts analysed, approximately 30–40% were classified as high-risk ($P(R_0(s) > 1) \geq 0.70$) under current climatic conditions. Concentrating acaricide distribution, veterinary surveillance, and community awareness programmes in this subset of districts rather than deploying uniform national coverage would reduce the required intervention footprint by approximately 60–70% while targeting the areas where climatic conditions most strongly support sustained CCHF transmission. The tiered decision framework described above provides a simple, model-derived basis for such prioritisation that requires only district-level climate data as input, making it operationally feasible within the existing data infrastructure of the Uganda Ministry of Health and the Ministry of Agriculture, Animal Industry and Fisheries. A full cost-effectiveness analysis incorporating unit costs of acaricide treatment per livestock head, cost per case averted, and health system capacity constraints is identified as an important direction for future work and would benefit from collaboration with health economists and the Uganda One Health platform (Zalwango et al., 2024).

V. LIMITATIONS OF THE STUDY

A limitation of the present study is that spatial heterogeneity is represented through climate-dependent parameterization at the district level rather than through explicit spatial transmission mechanisms. The model does not incorporate host mobility, livestock movement, tick dispersal, or diffusion processes between districts. Consequently, the generated maps should be interpreted as indicators of geographically varying transmission potential rather than predictions of spatial spread. Future work could extend the framework by incorporating movement networks or reaction diffusion processes to explicitly model disease propagation across regions.

A further limitation of the present model is that recruitment and natural mortality rates for livestock (π_L, μ_L) and humans (π_H, μ_H) are treated as fixed constants rather than climate-dependent quantities. In reality, livestock reproductive cycles and neonatal mortality may exhibit seasonal variation linked to rainfall and pasture availability, while human mortality may be indirectly influenced by climate-sensitive health determinants. Incorporating seasonally varying demographic rates for livestock and humans would require empirical data on seasonal birth, death, and migration rates at district level in Uganda, which are currently unavailable at the temporal and spatial resolution required by this model. Furthermore, the sensitivity analysis presented in Section III.G demonstrates that π_L and μ_L have relatively modest influence on R_0 compared with tick parameters (PRCC values below 0.35 in absolute value), suggesting that the omission of climate-driven demographic variation in these populations does not substantially alter the principal conclusions regarding climate-driven transmission dynamics. Future work incorporating district-level demographic surveillance data could extend the framework to include seasonally varying host demographic rates.

A further limitation concerns the temporal resolution of the climate inputs. ERA5-Land reanalysis data were obtained at daily temporal resolution, whereas tick physiological processes, particularly questing activity, desiccation survival during off-host periods, and developmental stage transitions, respond to sub-daily microclimatic variability at hourly scales (Randolph and Rogers, 2007; Estrada-Peña, Martínez Avilés and Muñoz Reoyo, 2011). The use of daily aggregated temperature and vapor pressure deficit values may smooth out extreme diurnal conditions that influence tick population dynamics, potentially leading to underestimation of variability in climate-driven transmission rates during periods of high thermal or desiccation stress. Future work incorporating hourly microclimate data, where available, would improve

the biological realism of the tick lifecycle functions and reduce this source of model uncertainty.

VI. CONCLUSION

This study presented a stochastic and climate-driven compartmental model for Crimean-Congo haemorrhagic fever (CCHF) transmission involving ticks, livestock, and humans in Uganda. The results demonstrate that climatic conditions, particularly temperature and vapor pressure deficit, strongly influence tick development, survival, and activity, thereby affecting transmission intensity across temporal and spatial scales. The stochastic formulation reproduced biologically realistic fluctuations and highlighted the role of environmental uncertainty in the persistence and extinction of infection. The spatial analysis further revealed significant heterogeneity across districts, with several locations exhibiting elevated transmission potential. These findings emphasize the importance of integrating climatic variability into epidemiological models for improved disease surveillance and intervention planning. From a public health perspective, the results suggest that surveillance and control measures should consider both seasonal and spatial patterns of vector activity. Prioritizing high-risk districts and critical climatic periods may improve response efficiency. Despite limitations related to the absence of explicit spatial diffusion mechanisms and incomplete surveillance data, the study provides a practical and biologically meaningful framework for understanding CCHF transmission. Overall, the integration of stochastic processes, climate-driven tick dynamics, and spatial analysis represents an important contribution toward environmentally informed surveillance and control strategies for vector-borne diseases in Uganda and provides a useful foundation for future climate-informed CCHF preparedness and model calibration.

AUTHOR CONTRIBUTIONS

P. G. Kpatchana: Conceptualization, methodology, mathematical modelling, software implementation, formal analysis, numerical simulations, visualization, writing original draft preparation. **J. Aduda**: Supervision, methodology review, manuscript review and editing. **K. M. Agboka**: Co-Supervision, climate data guidance, spatial analysis review, manuscript review and editing.

ACKNOWLEDGMENTS

we gratefully acknowledge the Pan African University Institute for Basic Sciences, Technology and Innovation (PAUSTI), Kenya, for academic support throughout this research. The authors also appreciate the guidance and constructive comments provided during the development of this work.

FUNDING

This work was not funded.

CONFLICTS OF INTEREST

The authors declare that there is no conflict of interest regarding this article.

CODE AND DATA AVAILABILITY

The ERA5-Land reanalysis climate data used in this study are publicly available from the Copernicus Climate Data Store at https://cds.climate.copernicus.eu (Muñoz-Sabater et al., 2021; Soci et al., 2024). CHIRPS precipitation data are freely accessible at https://www.chc.ucsb.edu/data/chirps (Funk et al., 2015). Administrative district boundary data for Uganda at ADM2 level were obtained from publicly available geospatial repositories. The Python implementation of the Milstein numerical scheme, spatial risk analysis, Latin Hypercube Sampling sensitivity analysis, and Monte Carlo uncertainty propagation developed in this study are available from the corresponding author upon reasonable request. Numerical simulations were performed using Python 3.11 with the NumPy, SciPy, and Matplotlib libraries. Spatial data processing and district-level risk maps were generated using R (version 4.4.0) with geospatial analysis packages, including sf, terra, and ggplot2. No proprietary software was used in the analysis.

REFERENCES

Allen, L. J. S. (2008). An Introduction to Stochastic Epidemic Models. In F. Brauer; P. van den Driessche and J. Wu (eds.), Mathematical Epidemiology. Lecture Notes in Mathematics, 1945, 81–130. Berlin, Heidelberg: Springer.

Balinandi, S.; **S. Mulei**; **S. Whitmer**; **L. Nyakarahuka**; **C. M. Cossaboom**; **E. Shedroff**; **M. Morales-Betoulle**; **I. Krapiunaya**; **A. Tumusiime** and **J. Kyondo (2024).** Crimean-Congo hemorrhagic fever cases diagnosed during an outbreak of Sudan virus disease in Uganda, 2022–23. PLoS Neglected Tropical Diseases, 18(10), e0012595. https://doi.org/10.1371/journal.pntd.0012595

Bernard, C.; **P. Holzmuller**; **M. T. Bah**; **M. Bastien**; **B. Combes**; **F. Jori**; **V. Grosbois** and **L. Vial (2022).** Systematic Review on Crimean–Congo Hemorrhagic Fever Enzootic Cycle and Factors Favoring Virus Transmission: Special Focus on France, an Apparently Free-Disease Area in Europe. Frontiers in Veterinary Science, 9, 932304. https://doi.org/10.3389/fvets.2022.932304

Bhowmick, S.; **K. K. Kasi**; **J. Gethmann**; **S. Fischer**; **F. J. Conraths**; **I. M. Sokolov** and **H. H. K. Lentz (2022).** Ticks on the Run: A Mathematical Model of Crimean-Congo Haemorrhagic Fever (CCHF)—Key Factors for Transmission. Epidemiologia, 3(1), 116–134. https://doi.org/10.3390/epidemiologia3010010

Briere, J.-F. ; **P. Pracros**; **A.-Y. Le Roux** and **J.-S. Pierre (1999).** A novel rate model of temperature-dependent development for arthropods. Environmental Entomology, 28(1), 22–29.

Estrada-Peña, A. (2023). The Climate Niche of the Invasive Tick Species Hyalomma marginatum and Hyalomma rufipes (Ixodidae) with Recommendations for Modeling Exercises. Experimental and Applied Acarology, 89(2), 231–250.

Estrada-Peña, A.; **M. Martínez Avilés** and **M. J. Muñoz Reoyo (2011).** A Population Model to Describe the Distribution and Seasonal Dynamics of the Tick Hyalomma marginatum in the Mediterranean Basin. Transboundary and Emerging Diseases, 58(3), 213–223. https://doi.org/10.1111/j.1865-1682.2010.01198.x

Funk, C.; **P. Peterson**; **M. Landsfeld**; **D. Pedreros**; **J. Verdin**; **S. Shukla**; **G. Husak**; **J. Rowland**; **L. Harrison** and **A. Hoell (2015).** The Climate Hazards Infrared Precipitation with Stations—A New Environmental Record for Monitoring Extremes. Scientific Data, 2(1), 150066. https://doi.org/10.1038/sdata.2015.66

Hethcote, H. W. (2000). The Mathematics of Infectious Diseases. SIAM Review, 42(4), 599–653. https://doi.org/10.1137/S0036144500371907

Hoch, T.; **E. Breton** and **Z. Vatansever (2018).** Dynamic Modeling of Crimean Congo Hemorrhagic Fever Virus (CCHFV) Spread to Test Control Strategies. Journal of Medical Entomology, 55(5), 1124–1132.

Khasminskii, R. (2012). Stability of Stochastic Differential Equations. In Stochastic Stability of Differential Equations, 145–176. Berlin, Heidelberg: Springer. https://doi.org/10.1007/978-3-642-23280-0

Kloeden, P. E. and **E. Platen (1992).** Numerical Solution of Stochastic Differential Equations. Berlin, Heidelberg: Springer.

Kriesel, A.; **M. Meyer** and **G. Peterson (2009).** Mathematical Modeling of Tick-Borne Encephalitis in Humans. Journal of Undergraduate Research at Minnesota State University, Mankato, 9(1), 9–16.

LaSalle, J. P. (1976). Stability Theory and Invariance Principles. In Dynamical Systems, 211–222. New York: Academic Press (Elsevier).

Mao, X. (2007). Stochastic Differential Equations and Applications. 2nd Edition. Oxford: Elsevier.

Matser, A.; **N. Hartemink**; **H. Heesterbeek**; **A. Galvani** and **S. Davis (2009).** Elasticity Analysis in Epidemiology: An Application to Tick-Borne Infections. Ecology Letters, 12(12), 1298–1305.

Mondal, M. K.; **M. Hanif** and **M. H. A. Biswas (2017).** A Mathematical Analysis for Controlling the Spread of Nipah Virus Infection. International Journal of Modelling and Simulation, 37(3), 185–197.

Mpeshe, S. C.; **H. Haario** and **J. M. Tchuenche (2011).** A Mathematical Model of Rift Valley Fever with Human Host. Acta Biotheoretica, 59(3–4), 231–250. https://doi.org/10.1007/s10441-011-9132-2

Muñoz-Sabater, J.; **E. Dutra**; **A. Agustí-Panareda**; **C. Albergel**; **G. Arduini**; **G. Balsamo**; **S. Boussetta**; **M. Choulga**; **S. Harrigan** and **H. Hersbach (2021).** ERA5-Land: A State-of-the-Art Global Reanalysis Dataset for Land Applications. Earth System Science Data, 13(9), 4349–4383. https://doi.org/10.5194/essd-13-4349-2021

Ogden, N. H.; **S. Mechai** and **G. Margos (2013).** Changing Geographic Ranges of Ticks and Tick-Borne Pathogens: Drivers, Mechanisms and Consequences for Pathogen Diversity. Frontiers in Cellular and Infection Microbiology, 3, 46. https://doi.org/10.3389/fcimb.2013.00046

Omoga, D. C. A.; **D. P. Tchouassi**; **M. Venter**; **E. O. Ogola**; **J. Osalla**; **A. Kopp**; **I. Slothouwer**; **B. Torto**; **S. Junglen** and **R. Sang (2023).** Transmission Dynamics of Crimean–Congo Haemorrhagic Fever Virus (CCHFV): Evidence of Circulation in Humans, Livestock, and Rodents in Diverse Ecologies in Kenya. Viruses, 15(9), 1891. https://doi.org/10.3390/v15091891

Randolph, S. E. and **D. J. Rogers (2007).** Ecology of Tick-Borne Disease and the Role of Climate. In O. Ergonul and C. A. Whitehouse (eds.), Crimean-Congo Hemorrhagic Fever: A Global Perspective, 167–186. Dordrecht: Springer.

Schuster, I.; **M. Mertens**; **S. Mrenoshki**; **C. Staubach**; **C. Mertens**; **F. Bruning**; **K. Wernike**; **S. Hechinger**; **K. Berxholi** and **D. Mitrov (2016).** Sheep and Goats as Indicator Animals for the Circulation of CCHFV in the Environment. Experimental and Applied Acarology, 68(3), 337–346.

Shayan, S.; **M. Bokaean**; **M. R. Shahrivar** and **S. Chinikar (2015).** Crimean-Congo Hemorrhagic Fever. Laboratory Medicine, 46(3), 180–189. https://doi.org/10.1309/LMN1P2FRZ7BKZSCO

Soci, C.; **H. Hersbach**; **A. Simmons**; **P. Poli**; **B. Bell**; **P. Berrisford**; **A. Horányi; J. Muñoz-Sabater**; **J. Nicolas** and **R. Radu (2024).** The ERA5 Global Reanalysis from 1940 to 2022. Quarterly Journal of the Royal Meteorological Society, 150(764), 4014–4048. https://doi.org/10.1002/qj.4861

Sutton, A. J.; **T. Karagenc**; **S. Bakirci**; **H. Sarali**; **G. Pekel** and **G. F. Medley (2012).** Modelling the Transmission Dynamics of Theileria annulata: Model Structure and Validation for the Turkish Context. Parasitology, 139(4), 441–453.

van den Driessche, P. and **J. Watmough (2002).** Reproduction Numbers and Sub-Threshold Endemic Equilibria for Compartmental Models of Disease Transmission. Mathematical Biosciences, 180(1–2), 29–48. https://doi.org/10.1016/S0025-5564(02)00108-6

World Health Organization (2025). Crimean–Congo Haemorrhagic Fever. Available from: https://www.who.int/news-room/fact-sheets/detail/crimean-congo-haemorrhagic-fever

Zalwango, J. F.; **P. King**; **M. G. Zalwango; H. N. Naiga**; **R. Akunzirwe**; **F. Monje**; **R. Migisha**; **L. Bulage**; **D. Kadobera** and **J. Kyondo (2024).** Another Crimean-Congo Hemorrhagic Fever Outbreak in Uganda: Ongoing Challenges with Prevention, Detection, and Response. IJID One Health, 2, 100019.

APPENDIX I

Positivity of the System

Proposition

The stochastic CCHF transmission system remains strictly positive for all $t > 0$ provided the initial conditions satisfy

$$T_S(0),\ T_E(0),\ T_I(0),\ L_S(0),\ L_E(0),\ L_I(0),$$

$$L_R(0),\ H_S(0),\ H_E(0),\ H_I(0),\ H_R(0) > 0$$

Applying Itô's lemma to the logarithmic transformation of a generic state variable $X(t)$ gives

$$d(\ln X) = \frac{1}{X}\,dX - \frac{1}{2X^2}(dX)^2$$

Since the drift and diffusion coefficients are locally Lipschitz and the stochastic perturbation preserves positivity, it follows that the logarithmic trajectories remain finite for all $t > 0$. Therefore,

$$X(t) > 0, \qquad t > 0$$

for all state variables of the system. □

APPENDIX II

Derivation of the Basic Reproduction Number

In this appendix, the basic reproduction number (R_0) of the deterministic CCHF model is derived using the next-generation matrix method. The infected-state vector is defined as

$$x = (T_E, T_I, L_E, L_I, H_E, H_I)^T$$

The infected subsystem is given by

$$\frac{dT_E}{dt} = \frac{\sigma_1 T_S L_I}{N_L} + \frac{\sigma_2 T_S T_I}{N_T} - (\mu_T + e_T)T_E$$

$$\frac{dT_I}{dt} = \frac{\varepsilon \pi_T T_I}{N_T} + e_T T_E - \mu_T T_I$$

$$\frac{dL_E}{dt} = \frac{\sigma_3 L_S T_I}{N_T} - (e_L + \mu_L)L_E$$

$$\frac{dL_I}{dt} = e_L L_E - (\alpha_L + \mu_L)L_I$$

$$\frac{dH_E}{dt} = \frac{\sigma_4 H_S T_I}{N_T} + \frac{\sigma_5 H_S L_I}{N_L} + \frac{\sigma_6 H_S H_I}{N_H} - (e_H + \mu_H)H_E$$

$$\frac{dH_I}{dt} = e_H H_E - (\alpha_H + \mu_H + \delta_H)H_I$$

Step 1: Disease-free equilibrium

At the disease-free equilibrium, all infected compartments vanish:

$$T_E *= T_I *= L_E *= L_I *= H_E *= H_I *= 0.$$

With these values we have:

$$T_S^* = \frac{\pi_T}{\mu_T}, \qquad L_S^* = \frac{\pi_L}{\mu_L}, \qquad H_S^* = \frac{\pi_H}{\mu_H}$$

Hence

$$N_T^* = T_S^* = \frac{\pi_T}{\mu_T}, \qquad N_L^* = L_S^* = \frac{\pi_L}{\mu_L},$$

$$N_H^* = H_S^* = \frac{\pi_H}{\mu_H}$$

Therefore,

$$\frac{T_S^*}{N_T^*} = 1, \qquad \frac{T_S^*}{N_L^*} = \frac{\pi_T \mu_L}{\mu_T \pi_L},$$

$$\frac{L_S^*}{N_T^*} = \frac{\pi_L \mu_T}{\mu_L \pi_T}, \qquad \frac{H_S^*}{N_T^*} = \frac{\pi_H \mu_T}{\mu_H \pi_T},$$

$$\frac{H_S^*}{N_L^*} = \frac{\pi_H \mu_L}{\mu_H \pi_L}, \qquad \frac{H_S^*}{N_H^*} = 1$$

Step 2: Decomposition into new infection and transition terms

The infected subsystem is written as $x' = F(x) - V(x)$,where $F(x)$collects all mechanisms that produce new infections, horizontal transmission and, in the tick compartment, vertical transmission and $V(x)$collects progression, recovery, and mortality terms.

$$\mathbf{F}(x) = \begin{pmatrix} \frac{\sigma_1 T_S L_I}{N_L} + \frac{\sigma_2 T_S T_I}{N_T} \\ \frac{\varepsilon \pi_T T_I}{N_T} \\ \frac{\sigma_3 L_S T_I}{N_T} \\ 0 \\ \frac{\sigma_4 H_S T_I}{N_T} + \frac{\sigma_5 H_S L_I}{N_L} + \frac{\sigma_6 H_S H_I}{N_H} \\ 0 \end{pmatrix}$$

$$\mathbf{V}(x) = \begin{pmatrix} (\mu_T + e_T)T_E \\ \mu_T T_I - e_T T_E \\ (e_L + \mu_L)L_E \\ (\alpha_L + \mu_L)L_I - e_L L_E \\ (e_H + \mu_H)H_E \\ (\alpha_H + \mu_H + \delta_H)H_I - e_H H_E \end{pmatrix}$$

Step 3: Construction of the matrices F and V

$$\frac{\partial}{\partial T_I}\left(\frac{\varepsilon \pi_T T_I}{N_T}\right)\Big|_{\text{DFE}} = \frac{\varepsilon \pi_T}{N_T^*} = \varepsilon \mu_T$$

All remaining entries follow from differentiating the horizontal-transmission terms as before. With $a = \sigma_1 \pi_T \mu_L/(\mu_T \pi_L)$,

$$b = \sigma_3 \pi_L \mu_T/(\mu_L \pi_T), c = \sigma_4 \pi_H \mu_T/(\mu_H \pi_T),$$

$d = \sigma_5 \pi_H \mu_L/(\mu_H \pi_L)$:

$$F = \begin{pmatrix} 0 & \sigma_2 & 0 & a & 0 & 0 \\ 0 & \varepsilon\mu_T & 0 & 0 & 0 & 0 \\ 0 & b & 0 & 0 & 0 & 0 \\ 0 & 0 & 0 & 0 & 0 & 0 \\ 0 & c & 0 & d & 0 & \sigma_6 \\ 0 & 0 & 0 & 0 & 0 & 0 \end{pmatrix}$$

$$V = \begin{pmatrix} \mu_T + e_T & 0 & 0 & 0 & 0 & 0 \\ -e_T & \mu_T & 0 & 0 & 0 & 0 \\ 0 & 0 & e_L + \mu_L & 0 & 0 & 0 \\ 0 & 0 & -e_L & \alpha_L + \mu_L & 0 & 0 \\ 0 & 0 & 0 & 0 & e_H + \mu_H & 0 \\ 0 & 0 & 0 & 0 & -e_H & \alpha_H + \mu_H + \delta_H \end{pmatrix}$$

Step 4: Inverse of V

V is a block diagonal, $V = diag(V_T, V_L, V_H)$, with

$$V_T = \begin{pmatrix} \mu_T + e_T & 0 \\ -e_T & \mu_T \end{pmatrix},$$

$$V_L = \begin{pmatrix} e_L + \mu_L & 0 \\ -e_L & \alpha_L + \mu_L \end{pmatrix},$$

$$V_H = \begin{pmatrix} e_H + \mu_H & 0 \\ -e_H & \alpha_H + \mu_H + \delta_H \end{pmatrix}$$

For a lower triangular matrix $M = \begin{bmatrix} [a, 0], \\ [-b, c] \end{bmatrix}, M^{-1} = \begin{bmatrix} [1/a, 0], \\ [b/(ac), 1/c] \end{bmatrix}$.

Therefore,

$$V_T^{-1} = \begin{pmatrix} \frac{1}{\mu_T + e_T} & 0 \\ \frac{e_T}{\mu_T(\mu_T + e_T)} & \frac{1}{\mu_T} \end{pmatrix},$$

$$V_L^{-1} = \begin{pmatrix} \frac{1}{e_L + \mu_L} & 0 \\ \frac{e_L}{(\alpha_L + \mu_L)(e_L + \mu_L)} & \frac{1}{\alpha_L + \mu_L} \end{pmatrix},$$

$$V_H^{-1} = \begin{pmatrix} \frac{1}{e_H + \mu_H} & 0 \\ \frac{e_H}{(\alpha_H + \mu_H + \delta_H)(e_H + \mu_H)} & \frac{1}{\alpha_H + \mu_H + \delta_H} \end{pmatrix}$$

and $V^{-1} = diag({V_T}^{-1}, {V_L}^{-1}, {V_H}^{-1})$.

Step 5: Computation of K = FV⁻¹

$$K = \begin{pmatrix} \frac{\sigma_2 e_T}{\mu_T(\mu_T + e_T)} & \frac{\sigma_2}{\mu_T} & \frac{a\, e_L}{(\alpha_L + \mu_L)(e_L + \mu_L)} & \frac{a}{\alpha_L + \mu_L} & 0 & 0 \\ \frac{\varepsilon e_T}{\mu_T + e_T} & \varepsilon & 0 & 0 & 0 & 0 \\ \frac{b\, e_T}{\mu_T(\mu_T + e_T)} & \frac{b}{\mu_T} & 0 & 0 & 0 & 0 \\ 0 & 0 & 0 & 0 & 0 & 0 \\ \frac{c\, e_T}{\mu_T(\mu_T + e_T)} & \frac{c}{\mu_T} & \frac{d\, e_L}{(\alpha_L + \mu_L)(e_L + \mu_L)} & \frac{d}{\alpha_L + \mu_L} & \frac{\sigma_6 e_H}{(\alpha_H + \mu_H + \delta_H)(e_H + \mu_H)} & \frac{\sigma_6}{\alpha_H + \mu_H + \delta_H} \\ 0 & 0 & 0 & 0 & 0 & 0 \end{pmatrix}$$

Step 6: Characteristic polynomial

Since rows 4 and 6 vanish identically, λ=0 is an eigenvalue with eigenvectors e_4 and e_6. Setting $v_4 = v_6 = 0$, the system decouples into a human-transmission block (row 5) and a tick–livestock block spanning T_E, T_I, L_E(rows 1–3). Define

$$k_{11} = \frac{\sigma_2 e_T}{\mu_T(\mu_T + e_T)}, \quad k_{12} = \frac{\sigma_2}{\mu_T},$$

$$k_{13} = \frac{a\, e_L}{(\alpha_L + \mu_L)(e_L + \mu_L)}, \quad k_{21} = \frac{\varepsilon e_T}{\mu_T + e_T},$$

$$k_{22} = \varepsilon, \quad k_{31} = \frac{b\, e_T}{\mu_T(\mu_T + e_T)}, \quad k_{32} = \frac{b}{\mu_T}$$

A direct check shows $k_{12}k_{21} = k_{11}k_{22}$and $k_{21}k_{32} = k_{22}k_{31}$ (row 2 of the tick sub-block is proportional to row 1, since $k_{21}/k_{11} = k_{22}/k_{12} = \varepsilon\mu_T/\sigma_2$).Using these identities, the 3×3 characteristic polynomial of the tick–livestock block reduces to

$$\lambda[\lambda^2 - (k_{11} + \varepsilon)\lambda - k_{13}k_{31}] = 0$$

where

$$k_{13}k_{31} = ab \cdot \frac{e_T e_L}{\mu_T(\mu_T + e_T)(\alpha_L + \mu_L)(e_L + \mu_L)} = \frac{\sigma_1\sigma_3 e_T e_L}{\mu_T(\mu_T + e_T)(\alpha_L + \mu_L)(e_L + \mu_L)} =: D$$

D depends only on the tick–livestock coupling parameters σ_1, σ_3, and is therefore identical to the value obtained without the vertical-transmission correction. Together with the two trivial zero eigenvalues from rows 4 and 6, and writing $k_{55} = \sigma_6 e_H/\big((e_H + \mu_H)(\alpha_H + \mu_H + \delta_H)\big)$

for the human block, the full characteristic polynomial of K is

$$\det(\lambda I - K) = \lambda^3(\lambda - k_{55})[\lambda^2 - (k_{11} + \varepsilon)\lambda - D]$$

Step 7: Eigenvalues of K

From the λ^3 factor: $\lambda_1 = \lambda_2 = \lambda_3 = 0$. From the human-to-human block: $\lambda_4 = k_{55}$. From the tick–livestock block:

$$\lambda_{5,6} = \frac{(k_{11}+\varepsilon) \pm \sqrt{(k_{11}+\varepsilon)^2 + 4D}}{2}$$

So

$$\text{Spec}(K) = \left\{0,0,0,\ \frac{\sigma_6 e_H}{(e_H+\mu_H)(\alpha_H+\mu_H+\delta_H)},\ \frac{(k_{11}+\varepsilon)+\sqrt{(k_{11}+\varepsilon)^2+4D}}{2},\ \frac{(k_{11}+\varepsilon)-\sqrt{(k_{11}+\varepsilon)^2+4D}}{2}\right\}$$

This accounts for exactly six eigenvalues with no multiplicity ambiguity, three zero eigenvalues, one human-pathway eigenvalue, and two tick–livestock eigenvalues, consistent with the dimension of K.

Step 8: Spectral radius

The basic reproduction number is the spectral radius of the next-generation matrix, $R_0 = \rho(FV^{-1})$. The zero eigenvalues do not contribute. Both remaining nonzero eigenvalues are positive, so

$$R_0 = \max\{R_{0H}, R_{0T}\}$$

$$R_{0H} = \frac{\sigma_6 e_H}{(e_H+\mu_H)(\alpha_H+\mu_H+\delta_H)}$$

$$R_{0T} = \frac{A+\sqrt{A^2+4D}}{2},$$

$$A = \frac{\sigma_2 e_T}{\mu_T(\mu_T+e_T)} + \varepsilon,$$

$$D = \frac{\sigma_1\sigma_3 e_T e_L}{\mu_T(\mu_T+e_T)(\alpha_L+\mu_L)(e_L+\mu_L)}$$

R_{0H} represents the reproduction potential from direct human-to-human transmission. R_{0TL} represents the reproduction potential generated by the coupled tick–livestock cycle, with vertical transmission now entering as a dimensionless additive contribution ε rather than the population-scaled term $\varepsilon\pi_T/\mu_T$ obtained under the earlier formulation. Since sustained transmission can be maintained through either pathway, the overall reproduction number is determined by the larger of the two components.

This completes the derivation. □

STOCHASTIC EXTINCTION OF THE DISEASE

Theorem

Let

$$Z(t) = T_I(t) + L_I(t) + H_I(t)$$

denote the total infectious population of the stochastic CCHF model. Assume that all model solutions remain positive for (t\ge0).

Define the Lyapunov function

$$V(Z) = \ln Z\,.$$

If the upper Lyapunov exponent

$$\lambda = \limsup_{t\to\infty} \frac{1}{t} \ln Z\,(t)$$

satisfies

$$\lambda < 0,$$

then

$$\lim_{t\to\infty} Z(t) = 0 \qquad \text{almost surely.}$$

Consequently,

$$T_I(t),\quad L_I(t),\quad H_I(t) \to 0 \qquad \text{almost surely,}$$

and the disease becomes extinct.

Proof

Define

$$Z(t) = T_I(t) + L_I(t) + H_I(t).$$

From the stochastic model,

APPENDIX III

$$dT_I = \left[e_T T_E - \mu_T T_I + \frac{\varepsilon\pi_T T_I}{N_T}\right]dt + \eta_{TI} T_I\, dW_3$$

$$dL_I = (e_L L_E - (\alpha_L+\mu_L)L_I)dt + \eta_{L_I} L_I\, dW_6,$$

$$dH_I = (e_H H_E - (\alpha_H+\mu_H+\delta_H)H_I)dt + \eta_{H_I} H_I\, dW_{10}.$$

Adding the three equations yields

$$dZ = b(Z,t)\,dt + \eta_{T_I} T_I\, dW_3 + \eta_{L_I} L_I\, dW_6 + \eta_{H_I} H_I\, dW_{10},$$

where

$$b(Z,t) = e_T T_E + e_L L_E + e_H H_E - \mu_T T_I - (\alpha_L+\mu_L)L_I - (\alpha_H+\mu_H+\delta_H)H_I + \frac{\varepsilon\pi_T T_I}{N_T}$$

Applying Itô's formula to

$$V(Z) = \ln Z\,,$$

gives

$$dV(Z) = \frac{1}{Z}dZ - \frac{1}{2Z^2}(dZ)^2.$$

Since the Wiener processes are independent,

$$(dZ)^2 = \left(\eta_{T_I}^2 T_I^2 + \eta_{L_I}^2 L_I^2 + \eta_{H_I}^2 H_I^2\right)dt.$$

Therefore,

$$dV(Z) = \left[\frac{b(Z,t)}{Z} - \frac{\eta_{T_I}^2 T_I^2 + \eta_{L_I}^2 L_I^2 + \eta_{H_I}^2 H_I^2}{2Z^2}\right]dt + dM(t),$$

where

$$dM(t) = \frac{\eta_{T_I} T_I}{Z} dW_3 + \frac{\eta_{L_I} L_I}{Z} dW_6 + \frac{\eta_{H_I} H_I}{Z} dW_{10}$$

is a martingale term.

Integrating from (0) to (t),

$$\ln Z(t) = \ln Z(0) + \int_0^t \left[\frac{b(Z,s)}{Z} - \frac{\eta_{T_I}^2 T_I^2 + \eta_{L_I}^2 L_I^2 + \eta_{H_I}^2 H_I^2}{2Z^2} \right] ds + M(t).$$

Dividing by (t),

$$\frac{\ln Z(t)}{t} = \frac{\ln Z(0)}{t} + \frac{1}{t}\int_0^t \left[\frac{b(Z,s)}{Z} - \frac{\eta_{T_I}^2 T_I^2 + \eta_{L_I}^2 L_I^2 + \eta_{H_I}^2 H_I^2}{2Z^2} \right] ds + \frac{M(t)}{t}.$$

By the strong law of large numbers for continuous martingales,

$$\lim_{t\to\infty} \frac{M(t)}{t} = 0 \qquad \text{almost surely.}$$

Also,

$$\lim_{t\to\infty} \frac{\ln Z(0)}{t} = 0.$$

Hence,

$$\lambda = \limsup_{t\to\infty} \frac{1}{t}\int_0^t \left[\frac{b(Z,s)}{Z} - \frac{\eta_{T_I}^2 T_I^2 + \eta_{L_I}^2 L_I^2 + \eta_{H_I}^2 H_I^2}{2Z^2} \right] ds.$$

If

$$\lambda < 0,$$

then there exists a constant (c>0) such that

$$\ln Z(t) \le -ct$$

for sufficiently large (t). Consequently,

$$Z(t) \le e^{-c} \to 0 \qquad (t \to \infty).$$

Since

$$0 \le T_I(t), L_I(t), H_I(t) \le Z(t),$$

it follows that

$$T_I(t) \to 0, \qquad L_I(t) \to 0, \qquad H_I(t) \to 0$$

almost surely.

Therefore, the disease becomes extinct.

□

APPENDIX IV

Foster–Lyapunov Condition for Stationary Distribution

Let

$$X(t) = (T_S, T_E, T_I, L_S, L_E, L_I, L_R, H_S, H_E, H_I, H_R)^T$$

denote the full state vector of the stochastic CCHF model. The system can be written as

$$dX(t) = b\big(X(t)\big)dt + G\big(X(t)\big)dW(t),$$

where (b(X)) is the drift vector and (G(X)) is the diffusion matrix.

Consider the Lyapunov function

$$V(X) = 1 + \|X\|^2 = 1 + \sum_{i=1}^{11} X_i^{2.}$$

This function is non-negative and satisfies

$$V(X) \to \infty \qquad \text{as} \qquad \|X\| \to \infty.$$

The infinitesimal generator applied to (V(X)) is

$$\mathcal{L}V(X) = 2X^T b(X) + \text{tr}\ (G(X)G(X)^T).$$

Since the diffusion matrix is diagonal,

$$G(X) = \text{diag}(\eta_i X_i), \qquad i = 1, \dots, 11,$$

we have

$$\text{tr}\ (G(X)G(X)^T) = \sum_{i=1}^{11} \eta_i^2 X_i^{2.}$$

Therefore,

$$\mathcal{L}V(X) = 2X^T b(X) + \sum_{i=1}^{11} \eta_i^2 X_i^{2.}$$

The drift vector (b(X)) contains recruitment terms, transmission terms, progression terms, recovery terms, and mortality/removal terms. Recruitment terms are bounded by at most linear growth, while mortality, recovery, and removal terms provide negative contributions for sufficiently large population sizes.

Using Young's inequality,

$$2ab \le \rho a^2 + \frac{1}{\rho} b^2, \qquad \rho > 0,$$

all positive linear terms can be bounded above by quadratic terms plus a positive constant. Consequently, there exist constants $(C_0 > 0)$ and $(m > 0)$ such that

$$2X^T b(X) \le -m\|X\|^2 + C_0,$$

provided that mortality, recovery, and removal dominate recruitment and amplification effects at large population sizes.

Substituting this estimate into the generator yields

$$\mathcal{L}V(X) \le -m\|X\|^2 + C_0 + \sum_{i=1}^{11} \eta_i^2 X_i^{2.}$$

Let

$$\eta_{\max}^2 = \max_{1\le i\le 1} \eta_i^2.$$

Then

$$\sum_{i=1}^{11} \eta_i^2 X_i^2 \le \eta_{\max}^2 \|X\|^2.$$

Therefore,

$$\mathcal{L}V(X) \le -(m - \eta_{\max}^2)\|X\|^2 + C_0.$$

Assume that

$$m > \eta_{\max}^2.$$

Define

$$c = m - \eta_{\max}^2 > 0.$$

Then

$$\mathcal{L}V(X) \le -c\|X\|^2 + C_0.$$

Since

$$V(X) = 1 + \|X\|^2,$$

we have

$$\|X\|^2 = V(X) - 1.$$

Substituting into the previous inequality gives

$$\mathcal{L}V(X) \le -c(V(X) - 1) + C_0.$$

Hence,

$$\mathcal{L}V(X) \le -cV(X) + (C_0 + c).$$

Let

$$d = C_0 + c.$$

Then

$$\mathcal{L}V(X) \le -cV(X) + d.$$

Therefore, outside a compact set (K),

$$\mathcal{L}V(X) \le -cV(X) + d, \qquad X \notin K.$$

This is the Foster–Lyapunov drift condition. Consequently, the stochastic process is positive recurrent and admits at least one invariant probability measure. Therefore, under the sufficient condition

$$m > \eta_{\max}^2,$$

the stochastic CCHF system admits a stationary distribution.

□

APPENDIX V

Uniqueness of the Stationary Distribution and Ergodicity

Lemma (Khasminskii, 2012). Let X(t) be a regular, temporally homogeneous Markov diffusion process satisfying

$dX = b(X)\,dt + G(X)\,dW$,with diffusion matrix

$\Sigma(X) = G(X)G(X)^T$.Suppose there exists a bounded open domain U $\subset \mathbb{R}_+^{11}$ with regular boundary such that

$\xi^T\Sigma(X)\xi \ge M|\xi|^2$, for all $X \in U$
and some constant $M > 0$, (E.1)

and suppose there exists a non-negative C² function V such that

$LV(X) < 0$, for all $X \in \mathbb{R}_+^{11} \setminus U$. (E.2)

Then the process admits a unique stationary distribution and is ergodic.

Step 1: Lyapunov function

Consider

$$V(X) = \sum_{i=1}^{11} (X_i - 1 - \ln X_i).$$

Since

$$X_i - 1 - \ln X_i \ge 0,$$

with equality only at X_i =1, and

$X_i - 1 - \ln X_i \to \infty$ as $X_i \to 0^+$or $X_i \to \infty$,the function V is coercive on the positive orthant: every sublevel set $\{X: V(X) < N\}$ is bounded and bounded away from the coordinate boundaries.

Step 2: Verification of condition (E.1)

The diffusion matrix is diagonal,

$\Sigma(X) = \mathrm{diag}(\eta_1^2 X_1^2, \dots, \eta_{11}^2 X_{11}^2)$.

For any compact sublevel set

$$U_N = \{X: V(X) < N\},$$

coercivity of V gives constants

$0 < \varepsilon_i(N) \le X_i \le R_i(N)$, $i = 1, \dots, 11$,

for all $X \in U_N$. Hence

$$\xi^T\Sigma(X)\xi \ge \left(\min_i \eta_i^2\, \varepsilon_i(N)^2\right)|\xi|^2,$$

so condition (E.1) holds with $M = min_i \eta_i{}^2 \varepsilon_i(N)^2$,

provided all eleven noise intensities η_i are nonzero.

Step 3: Behaviour near the boundary

For $g(u) = u - 1 - lnu$, Itô's formula gives

$$L[g(X_i)] = \left(1 - \frac{1}{X_i}\right) b_i(X) + \frac{1}{2}\eta_i^2.$$

itself bounded away from zero, so that as $X_i \to 0^+$ with the remaining coordinates held in the persistence region, $b_i(X)$ converges to a strictly positive limit and $L[g(X_i)] \to -\infty$.

Three representative cases illustrate the general pattern:

For exposed ticks, $b_{T_E}(X) = \sigma_1 T_S L_I/N_L + \sigma_2 T_S T_I/N_T$, which tends to $\sigma_1 T_S L_I/N_L + \sigma_2 T_S T_I/N_T > 0$as $T_E \to 0^+$,since T_S, L_I, T_I remain positive in the persistence region.

For exposed livestock, $b_{L_E}(X) = \sigma_3 L_S T_I/N_T - (e_L + \mu_L)L_E$, which tends to $\sigma_3 L_S T_I/N_T > 0$as $L_E \to 0^+$.

For exposed humans, $b_{H_E}(X) = \sigma_4 H_S T_I/N_T + \sigma_5 H_S L_I/N_L + \sigma_6 H_S H_I/N_H - (e_H + \mu_H)H_E$,which tends to $\sigma_4 H_S T_I/N_T + \sigma_5 H_S L_I/N_L + \sigma_6 H_S H_I/N_H > 0$ as $H_E \to 0^+$.

The same mechanism applies to every remaining compartment: $T_I, L_I, and\ H_I$ each receive positive inflow from their respective exposed class $(e_T T_E, e_L L_E, e_H H_E)$; L_R and H_R receive positive inflow from their respective infectious class $(\alpha_L L_I, \alpha_H H_I)$; and T_S, L_S, H_S receive the constant positive recruitment terms π_T, π_L, π_H, which never vanish. Hence

$LV(X) \to -\infty$ near every boundary face of the persistence set.

Step 4: Behaviour at infinity

Summing the drift equations over the three tick compartments, the internal transmission terms cancel and the vertical transmission terms combine to give

$T_S + T_E + T_I$: $\sum b_i(X) = \pi_T\left(1 + \frac{T_I}{N_T}\right) - \mu_T N_T \leq 2\pi_T - \mu_T N_T$, using $T_I/N_T \leq 1$.

Summing the four livestock compartments, the transmission terms cancel exactly and

$$L_S + L_E + L_I + L_R: \quad \sum b_i(X) = \pi_L - \mu_L N_L.$$

Summing the four human compartments, the transmission terms cancel and the disease-induced mortality term only strengthens the bound,

$$H_S + H_E + H_I + H_R: \quad \sum b_i(X) = \pi_H - \mu_H N_H - \delta_H H_I \leq \pi_H - \mu_H N_H.$$

Adding the three contributions,

$$\sum_i b_i(X) \leq (2\pi_T + \pi_L + \pi_H) - \mu_{\min}\|X\|_1,$$

where $\mu_{min} = min(\mu_T, \mu_L, \mu_H)$. Consequently,

$$LV(X) \leq C_1 - \mu_{\min}\|X\|_1$$

for the constant $C_1 = 2\pi_T + \pi_L + \pi_H + (1/2)\Sigma\eta_i^2$.

Therefore $LV(X) < 0$ for sufficiently large $\|X\|_1$, so condition (E.2) holds on the complement of a sufficiently large bounded domain U.

Step 5: Conclusion

Conditions (E.1) and (E.2) are satisfied. By Lemma E.1, the stochastic CCHF system possesses a unique stationary distribution in the persistence regime and is ergodic.

APPENDIX VI

STABILITY ANALYSIS OF THE DETERMINISTIC SYSTEM

1 Global Stability of the Disease-Free Equilibrium ($R_0 < 1$)

Let the disease-free equilibrium be

$$E^0 = (T_S^0, 0, 0, L_S^0, 0, 0, 0, H_S^0, 0, 0, 0),$$

where

$$T_S^0 = \frac{\pi_T}{\mu_T}, L_S^0 = \frac{\pi_L}{\mu_L}, H_S^0 = \frac{\pi_H}{\mu_H}.$$

Let $x = (T_E, T_I, L_E, L_I, H_E, H_I)^T$denote the infected-state vector. Near $E^0$the infected subsystem satisfies

$$\dot{x} = (F - V)\,x,$$

where $F$and $V$are the transmission and transition matrices derived in Appendix II.

The basic reproduction number is $R_0 = \rho(FV^{-1})$, where $\rho(\cdot)$denotes the spectral radius. Suppose $R_0 < 1$.

Since $F$is non-negative and $V$is a nonsingular M-matrix, the product $FV^{-1}$is non-negative with $\rho(FV^{-1}) < 1$. Consequently $(I - FV^{-1})$is an M-matrix, and by the theory of non-negative matrices there exists a strictly positive vector

$$q = (q_1, q_2, \ldots, q_6)^T > 0$$

satisfying

$$q^T FV^{-1} < q^T.$$

Multiplying on the right by Vgives $q^T F < q^T V$, and therefore

$$q^T(F - V) < 0,$$

Define the Lyapunov function

$$V_{\mathrm{DFE}} = q^T x.$$

Since $q > 0$and $x \geq 0$, we have $V_{\mathrm{DFE}} \geq 0$with equality if and only if $x = 0$. Differentiating along solutions:

$$\frac{dV_{\mathrm{DFE}}}{dt} = q^T\dot{x} = q^T(F - V)\,x \leq 0,$$

with equality only when $x = 0$. By LaSalle's invariance principle (LaSalle, 1976), every solution converges to E^0. Hence the disease-free equilibrium is globally asymptotically stable whenever $R_0 < 1$. □

F.2 Local Asymptotic Stability of the Endemic Equilibrium ($R_0 > 1$)

When $R_0 > 1$the deterministic model admits a unique endemic equilibrium

$$E^* = (T_S^*, T_E^*, T_I^*, L_S^*, L_E^*, L_I^*, L_R^*, H_S^*, H_E^*, H_I^*, H_R^*) \in \mathbb{R}_+^{11},$$

whose existence and uniqueness follow from the irreducibility of the infected subsystem and a fixed-point argument applied to the steady-state equations when $R_0 > 1$.

Let $J^* = DF(E^*)$denote the Jacobian of the deterministic system evaluated at E^*. Local asymptotic stability of $E^*$is equivalent, by Lyapunov's indirect method, to the condition that all eigenvalues of J^*have strictly negative real parts.

The Jacobian has the block structure

$$J^* = \begin{pmatrix} J_{SS} & J_{SI} \\ J_{IS} & J_{II} \end{pmatrix},$$

where $J_{SS}$and J_{II}correspond to the susceptible/recovered compartments $(T_S, L_S, L_R, H_S, H_R)$and the infected compartments $(T_E, T_I, L_E, L_I, H_E, H_I)$, respectively.

Susceptible and recovered block. $J_{SS}$is a lower-triangular matrix with diagonal entries

$$-\mu_T, -\mu_L, -\mu_L, -\mu_H, -(\alpha_H + \mu_H + \delta_H),$$

all of which are strictly negative. Its eigenvalues therefore have strictly negative real parts.

Infected block. At the endemic equilibrium the steady-state balance equations require that the net production of each infected class is exactly matched by its net removal. Any positive perturbation to an infected compartment increases the force of infection on the corresponding susceptible class, which is already depleted below the disease-free level X_S^0; this depleted susceptible pool reduces the effective transmission rate and drives the perturbation back toward E^*. Consequently, the infected-block sub-matrix $J_{II}$is stable, with all eigenvalues having strictly negative real parts. This conclusion is confirmed numerically at the baseline endemic parameterisation underlying the simulations presented in Section IV (R_0 = 2.42), for which the full Jacobian J* was evaluated directly at the corresponding endemic equilibrium E* and found to satisfy $max_k Re(\lambda_k(J*)) = -0.0059 < 0$ across all eleven eigenvalues, confirming local asymptotic stability for the parameter set used to generate the reported results. By Lyapunov's indirect method, the endemic equilibrium $E^*$is locally asymptotically stable whenever $R_0 > 1$.

Appendix VI concerns only the deterministic model. For the stochastic system, almost-sure extinction under the sub-threshold condition ($R_0 < 1$) is established in Appendix III via the Lyapunov exponent of the aggregated infectious process, while stochastic persistence and ergodicity in the super-threshold regime ($R_0 > 1$) are established via the Foster–Lyapunov drift condition in Appendix IV and Khasminskii's non-degeneracy criterion in Appendix V. The deterministic and stochastic results are therefore fully consistent: global convergence to E^0in the deterministic model corresponds to almost-sure stochastic extinction, and local stability of E^*corresponds to the existence of a unique stationary distribution concentrated near the endemic state.